



**HAL**  
open science

## A decade of GPS in Southeast Asia: Resolving Sundaland motion and boundaries

W. J. F. Simons, A. Socquet, C. Vigny, B. A. C. Ambrosius, S. Haji Abu, Chaiwat Promthong, C. Subarya, D. A. Sarsito, S. Matheussen, P. Morgan, et al.

► **To cite this version:**

W. J. F. Simons, A. Socquet, C. Vigny, B. A. C. Ambrosius, S. Haji Abu, et al.. A decade of GPS in Southeast Asia: Resolving Sundaland motion and boundaries. *Journal of Geophysical Research : Solid Earth*, 2007, 112, 10.1029/2005JB003868 . insu-03603183

**HAL Id: insu-03603183**

**<https://insu.hal.science/insu-03603183>**

Submitted on 9 Mar 2022

**HAL** is a multi-disciplinary open access archive for the deposit and dissemination of scientific research documents, whether they are published or not. The documents may come from teaching and research institutions in France or abroad, or from public or private research centers.

L'archive ouverte pluridisciplinaire **HAL**, est destinée au dépôt et à la diffusion de documents scientifiques de niveau recherche, publiés ou non, émanant des établissements d'enseignement et de recherche français ou étrangers, des laboratoires publics ou privés.

Copyright

## A decade of GPS in Southeast Asia: Resolving Sundaland motion and boundaries

W. J. F. Simons,<sup>1</sup> A. Socquet,<sup>1,9</sup> C. Vigny,<sup>2</sup> B. A. C. Ambrosius,<sup>1</sup> S. Haji Abu,<sup>3</sup> Chaiwat Promthong,<sup>4</sup> C. Subarya,<sup>5</sup> D. A. Sarsito,<sup>6</sup> S. Matheussen,<sup>1</sup> P. Morgan,<sup>7</sup> and W. Spakman<sup>8</sup>

Received 6 June 2005; revised 16 January 2007; accepted 2 March 2007; published 29 June 2007.

[1] A unique GPS velocity field that spans the entire Southeast Asia region is presented. It is based on 10 years (1994–2004) of GPS data at more than 100 sites in Indonesia, Malaysia, Thailand, Myanmar, the Philippines, and Vietnam. The majority of the horizontal velocity vectors have a demonstrated global accuracy of  $\sim 1$  mm/yr (at 95% confidence level). The results have been used to (better) characterize the Sundaland block boundaries and to derive a new geokinematic model for the region. The rotation pole of the undeformed core of the Sundaland block is located at  $49.0^{\circ}\text{N}$ – $94.2^{\circ}\text{E}$ , with a clockwise rotation rate of  $0.34^{\circ}/\text{Myr}$ . With respect to both geodetically and geophysically defined Eurasia plate models, Sundaland moves eastward at a velocity of  $6 \pm 1$  to  $10 \pm 1$  mm/yr from south to north, respectively. Contrary to previous studies, Sundaland is shown to move independently with respect to South China, the eastern part of Java, the island of Sulawesi, and the northern tip of Borneo. The Red River fault in South China and Vietnam is still active and accommodates a strike-slip motion of  $\sim 2$  mm/yr. Although Sundaland internal deformation is generally very small (less than 7 nanostrain/yr), important accumulation of elastic deformation occurs along its boundaries with fast-moving neighboring plates. In particular in northern Sumatra and Malaysia, inland-pointing trench-perpendicular residual velocities were detected prior to the megathrust earthquake of 26 December 2004. Earlier studies in Sumatra already showed this but underestimated the extent of the deformation zone, which reaches more than 600 km away from the trench. This study shows that only a regional Southeast Asia network spanning thousands of kilometers can provide a reference frame solid enough to analyze intraplate and interplate deformation in detail.

**Citation:** Simons, W. J. F., et al. (2007), A decade of GPS in Southeast Asia: Resolving Sundaland motion and boundaries, *J. Geophys. Res.*, 112, B06420, doi:10.1029/2005JB003868.

### 1. Introduction

[2] The Sundaland block (Figure 1) covers a large part of present-day Southeast Asia that includes Indochina (Cambodia, Laos, Vietnam), Thailand, Peninsular Malaysia, Sumatra, Borneo, Java, and the shallow seas located in between (Sunda shelf). It is mostly surrounded by highly

active subduction zones, in which (clockwise from east to west) the adjacent Philippine, Australian, and Indian plates submerge. To the north, Sundaland is bounded by the southeastern part of the India-Eurasia collision zone and the South China (or Yantze) block. While the vast majority of seismicity in SE Asia occurs in these surrounding plate subduction and collision zones (Figure 1), Sundaland's interior is only affected by a very low rate of shallow seismicity. This suggests Sundaland presently moves as a coherent lithospheric block, although its geological origin clearly is not monolithic [*Hall and Morley*, 2004]. Unfortunately, reliable estimates of the interplate motions between Sundaland and the adjacent plates are difficult to obtain from seismic slip vectors alone.

[3] Is the Sundaland block (together with the South China and Amurian (North China) blocks) still part of (stable) Eurasian plate or does it move independently? This knowledge is important for the extensive studies of the Asian continental deformation initiated by analysis of satellite imagery [*Tapponnier and Molnar*, 1977] and geological and seismological data [*Molnar and Tapponnier*, 1978].

<sup>1</sup>Delft Institute of Earth Observation and Space Systems (DEOS), Delft University of Technology, Delft, Netherlands.

<sup>2</sup>École Normale Supérieure (ENS), Paris, France.

<sup>3</sup>Department of Survey and Mapping Malaysia (DSMM), Kuala Lumpur, Malaysia.

<sup>4</sup>Royal Thai Survey Department (RTSD), Bangkok, Thailand.

<sup>5</sup>National Coordination Agency for Surveys and Mapping (BAKOSURTANAL), Cibinong, Indonesia.

<sup>6</sup>Institute of Technology Bandung (ITB), Bandung, Indonesia.

<sup>7</sup>School of Computing, University of Canberra, Canberra, ACT, Australia.

<sup>8</sup>Faculty of Earth Sciences, University of Utrecht, Utrecht, Netherlands.

<sup>9</sup>Now at Institut de Physique du Globe de Paris (IPGP), Paris, France.

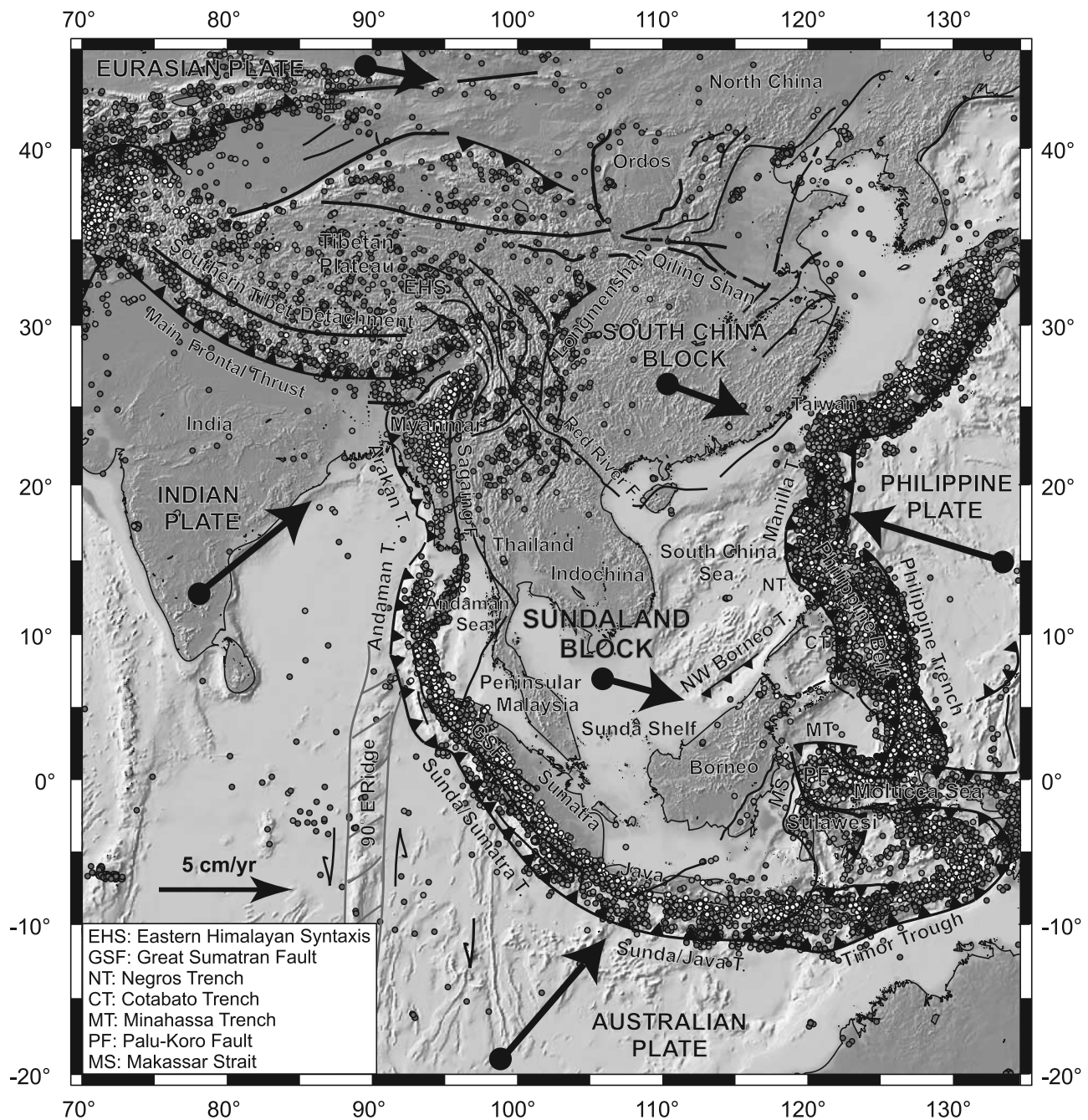


**Figure 1.** Topography, seismicity, main active faults, index of the geographical names used in this paper, and the approximate (absolute/ITRF2000) motions of the Eurasian, Indian, Australian, Philippine plates and the South China and Sundaland blocks, respectively, near and in SE Asia.

Over the past 3 decades various models have been proposed that explain this deformation either by viscous flow of a continuously deforming medium [e.g., England and Houseman, 1986; Houseman and England, 1993; England and Molnar, 1997] or by motion of rigid lithospheric blocks along narrow fault zones [e.g., Tapponnier et al., 1982; Avouac and Tapponnier, 1993; Peltzer and Saucier, 1996]. A well-defined Sundaland motion allows for better assessment and/or further improvement of these models.

[4] In the past the tectonic settings of Central and Southeast Asia were much less detailed, and Sundaland

was often considered as an extension of the Eurasian plate. However, subsequent geological and geophysical studies of the Indonesian Archipelago clearly recognized SE Asia (Sunda shelf) as a consistent tectonic entity that moves differently than Eurasia [Fitch, 1972; Cardwell and Isacks, 1978; Hamilton, 1979; Curray, 1989; McCaffrey, 1991; Hall and Nichols, 2002]. Confirmation of these observations only became possible during the 1990s with an important advance in space geodesy; the use of high precision GPS measurements to accurately determine crustal motions.

[5] Initial GPS results in SE Asia [e.g., *Tregoning et al.*, 1994; *Genrich et al.*, 1996] concluded that this region seemed to be part of the Eurasian plate. However, this was based on GPS measurements from relatively small local networks that were mainly located in plate deformation zones (Sumatra, Java, Sulawesi, Banda arc) that surround the Sundaland block. In contrast, the “Geodynamics of South and Southeast Asia” (GEODYSSSEA) network [*Wilson et al.*, 1998] includes ~40 GPS points systematically distributed over SE Asia and clearly confirmed Sundaland as a coherent block which moves with respect to Eurasia and is separated from the Siberian platform through a series of deforming and moving blocks [*Wilson et al.*, 1998; *Chamote-Rooke and Pichon*, 1999; *Simons et al.*, 1999; *Michel et al.*, 2001]. More recently published GPS studies also have defined an independently moving Sunda plate [*Sella et al.*, 2002; *Bock et al.*, 2003; *Kreemer et al.*, 2003].

[6] Although all GPS results in first-approximation indicate that SE Asia moves eastward at ~1 cm/yr relative to Siberia, there are still significant discrepancies in the definition of the Sundaland boundaries and (any) motion relative to Eurasia and South China. The higher level of accuracy required to resolve such motion can only be achieved with long time series of GPS data from a dense network. Therefore since 1998 the GPS network in SE Asia has been significantly expanded with both campaign sites and continuously operated stations. This was accomplished by carrying out new GPS surveys with local agencies and by data sharing (in the EU-ASEAN “Southeast Asia: Mastering Environmental Research with Geodetic Space Techniques” (SEAMERGES) project) with other European, Indonesian, Japanese, Malaysian, and Thai researchers. This resulted in a unique GPS data set which spans a full decade and includes data from more than 100 sites. All these data were (re-)processed, using the latest state-of-the-art processing techniques, to obtain GPS velocities in the International Terrestrial Reference Frame 2000 (ITRF2000) [*Altamimi et al.*, 2002].

[7] In this paper the GPS network and the data characteristics are described. This is followed by an explanation of the data analysis methodology and the mapping strategy. Then the paper focuses on the issue of more clearly defining the boundaries and internal deformation of the Sundaland block with GPS. Next, the resulting rotation vector for Sundaland and the consequences for its relative motion with respect to the neighboring plates are discussed. In this context, recently published, improved solutions for the Eurasian and South China rotation poles [*Calais et al.*, 2003; *Fernandes et al.*, 2003; *Shen et al.*, 2005] are of crucial importance. The body of this paper only contains the most important figures and tables. More information can be found in the electronic supplement of this paper and at <http://www.deos.tudelft.nl/~wims/sunda.html><sup>1</sup>.

## 2. GPS Network

[8] The analyzed network (Figure 2) is a densification of the 4000 by 4000 km GEODYSSSEA network that encompasses the major plate tectonic zones in SE Asia. The results

of *Michel et al.* [2001] from 3 GPS campaigns between 1994 and 1998 lacked sufficient density and accuracy to discriminate everywhere between stations on blocks and stations in deforming zones. Therefore in addition to remeasuring parts of the original network, the network was expanded in three regions (each boxed in Figure 2), with a total of ~60 points: six THAICA sites and six permanent GAME-T stations [*Takiguchi et al.*, 2000; *Iwakuni et al.*, 2004] in Thailand (Box 1), four new sites in Myanmar [*Vigny et al.*, 2003] (Box 1), 18 permanent MASS stations in Malaysia (Box 2), 20 new campaign sites and six permanent stations in Sulawesi (Box 3), and two permanent stations (Java and Sumatra) in Indonesia. The yearly contents of the GPS database, conforming to the above network layout, are presented in Table 1. Data was collected between 27 November 1994 and 25 December 2004. Points were measured 3 to 9 times in (multiple day) campaign-style or continuously for 5 to 7 years (Indonesia, Malaysia, and Thailand). Details on the deformation of the network due to the 2004 Sumatra-Andaman earthquake are in the work of *Vigny et al.* [2005].

[9] While it is the most dense network currently available for SE Asia, it also is an inhomogeneous network (both in spatial and in temporal sense). Therefore the main challenge is to derive a coherent and accurate velocity field in a global reference frame (ITRF2000). To assist frame definition, the SE Asia network was further extended with 31 globally distributed International GPS Service (IGS) sites. The IGS sites include 14 regional and 17 global stations (see inset of Figure 2 and IGS section in Table 1). Including only regional stations was inappropriate since the IGS network is sparse and inconsistent during the 10-year data span. Some stations also had time series too short to yield accurate reference frame positions and velocities.

## 3. GPS Data Analysis

[10] The dual frequency GPS data from the full network (SE Asia + global IGS) were uniformly (re)processed using the GIPSY-OASIS II software [*Blewitt et al.*, 1988] developed at the Jet Propulsion Laboratory (JPL). The Precise Point Positioning (PPP) strategy [*Zumberge et al.*, 1997] was applied since it ideally suits the large and inhomogeneous network in this paper. The PPP strategy requires consistent GPS orbits and clocks, which together with the Earth rotation parameters were retrieved from JPL. The different steps in the data analysis described below are important indicators of the claimed velocity field accuracy. Additional details are available in the electronic supplement of this paper.

### 3.1. Daily Solutions

[11] The GPS data were processed in daily batches with the PPP strategy. Each point position is based on the ionospheric free combination of the zero-differenced GPS observables at 5 minute intervals, with a cutoff elevation angle of 15 degrees. Tropospheric delays and gradients were stochastically estimated at each interval. Ocean loading effects were modeled according to *Scherneck* [1991]. To account for different GPS antennae, relative antenna phase center corrections were applied (National Geodetic Survey (NGS) [*Mader*, 1998]). The individual point positions were

<sup>1</sup>Auxiliary material data sets are available at <ftp://ftp.agu.org/apend/jb/2005/jb003868>. Other auxiliary material files are in the HTML.

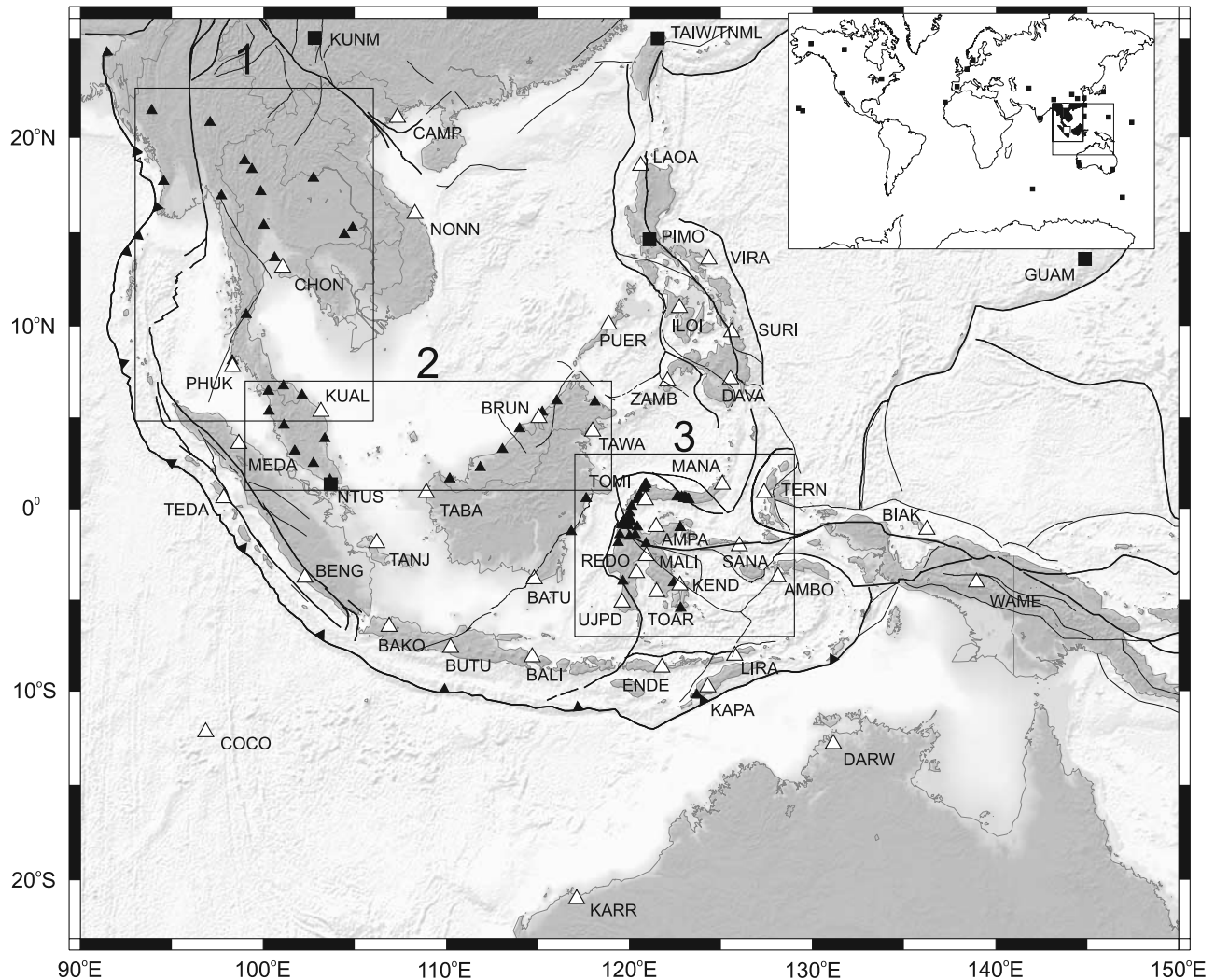


**Figure 2.** GPS network in SE Asia used in this study. Open triangles denote GEODYSSSEA points, while solid triangles represent new densification points. Permanent IGS stations are marked as solid squares. The three numbered boxes highlight distinct densification regions: (1) Thailand, (2) Malaysia, and (3) Sulawesi, Indonesia (detailed figures available in the electronic supplement). The inset shows a world map with the global network of IGS stations (solid squares) that was used to map the SE Asia solution into ITRF2000. The larger box outlines the region of the main panel of this figure. The smaller box zooms in on the Sundaland block.

merged into daily full-network solutions. Owing to the nature of PPP processing, the different station positions are modeled as uncorrelated. Nevertheless, the phase ambiguities can still be fixed to improve the position in east-west direction. This is the only processing step where GIPSY relies on double differencing. The large network requires an iterative (boot-strapping) ambiguity fixing scheme, which processes stations with shorter baselines first. This step also produces a full covariance matrix, which is advantageous in network combinations and reference frame transformations.

### 3.2. Multiday Solutions in ITRF2000

[12] The daily ambiguity-fixed solutions were combined into multiday averaged solutions using seven-parameter Helmert transformations, in order to condense the results and to facilitate the detection and down weighting of outliers. From 1998 onward, this combination was performed weekly when only the permanent GPS subnetworks were

active. During campaign periods (on average once per year), daily solutions were averaged over the campaign length, which varied from 1 to 3 weeks. The overall repeatability statistics of each combination solution were used to scale the formal errors in their variance/covariance matrices. Formal errors are typically underestimated in GPS processing results. Assigning realistic error estimates to the coordinates should result in more realistic velocity estimate uncertainties. In general, the daily coordinate repeatabilities are 2 and 4 mm for the north and east horizontal positions, respectively, and 9 mm for the height.

[13] The weekly/campaign fiducial-free network solutions were transformed into the ITRF2000 using the coordinates and velocities of a subset of 12 to 25 well determined global IGS stations to estimate seven-parameter Helmert transformations. The remaining IGS sites, including NTUS, BAKO, and PIMO in SE Asia, were adjusted along with the local network. In sequence, stations COCO,

**Table 1.** Overview of the Available Sites in the 1994–2004 GPS Database<sup>a</sup>

Description	Size	Year									
		1994	1996	1997	1998	1999	2000	2001	2002	2003	2004
GEODYSSSEA	40	39	40	14	38	4	10	4	9	6	3
Region 1											
THAICA	6	5	3	-	-	-	1	5	6	-	5
ENS	4	-	-	-	4	-	4	-	-	-	-
GAME-T	6	-	-	-	6*	5*	5*	3*	3*	3*	3*
Region 2											
MASS	18	-	-	-	9	15*	15*	17*	18*	18*	18*
Region 3											
GEODYSSSEA Sec.	16	-	6	7	7	4	8	8	12	12	10
BAKO monuments	6	-	-	1	1	4	5	4	6	6	6
BAKO permanent	7	-	1	2	2	3*	5*	5*	7*	7*	7*
IGS											
Local (SE Asia)	3	-	-	1	2*	3*	3*	3*	3*	3*	3*
Subtotal	106	44	50	25	69	38	56	49	64	55	55
IGS											
Regional + global	31	21	25	26	28*	28*	27*	28*	29*	28*	29*
Total	137	67	75	51	97	66	83	77	93	83	84

<sup>a</sup>The table shows the size of all the (sub)networks in each region (Figure 2), followed by the number of sites observed in each year. Numbers marked with an asterisk indicate that all the available permanent data was daily processed for that particular year (MASS, GAME-T, BAKO, and IGS permanent networks from 1999 to 2004).

KOKB, TSKB, GUAM, GOLD, FAIR, and KOSG were excluded when notable discontinuities occurred in their time series. The coordinate residuals at IGS stations indicate precision in ITRF2000 (at 95% confidence level) of 3–4 mm, 3–5 mm, and 10–14 mm in the north, east, and up components, respectively. The applied mapping technique facilitates future readjustments of the network in new ITRF solutions like the ITRF2005 that will be made available through the paper Web page (<http://www.deos.tudelft.nl/~wims/sunda.html>).

### 3.3. GPS Velocity Field

[14] From 1994 onward, the ~360 weekly/campaign GPS networks in ITRF2000 resulted in up to 10-year long position time series. Station velocities were extracted by linear regression, which implies steady-state motion. This was verified by analyzing the misfits with respect to the linear trends. Mostly only small offsets were observed, and overall the three-dimensional (3-D) root-mean-square (RMS) values are 3, 5, and 11 mm in north, east, and up, respectively. Some stations have less “smooth” time series, particularly in the high seismicity regions of Sulawesi and the Banda Arc. These sites may have experienced monument motion or aseismic events (e.g., the TOLI station in North Sulawesi), as neither large quakes nor data problems occurred. Elsewhere in the network, epochs clearly affected by seismicity were excluded (episodic sites) and position jumps were estimated (permanent sites).

[15] Additional tests were performed to verify both the transformations into ITRF2000 and the accuracy of the velocity estimates. For example, the velocity estimates for the well determined IGS stations agree with the ITRF2000 values within 1 and 2 mm/yr for the horizontal and vertical directions, respectively (table included in electronic supplement). This is a noteworthy result, because nowhere have coordinates or velocities been constrained. To illustrate the robustness and precision of the analysis approach, the time series for the station KUAL in Malaysia is shown in Figure 4. Originally a GEODYSSSEA campaign point, it was equipped with a permanent receiver at the end of 1998. The 1997 campaign measurement is clearly an outlier, most

probably due to a wrongly documented GPS antenna type or a misaligned antenna setup.

[16] The uncertainties of the SEAMERGES GPS velocity field (at 95% confidence level) are ~1 mm/yr at continuously operating sites and 1 to 4 mm/yr at campaign sites. These were obtained by increasing the formal errors of all estimates by individual factors determined from the weighted root-mean-square (WRMS) fit and length of each time series. Hereby it is assumed that the uncertainty of the linear trend estimate is bounded by  $-WRMS$  at the start and  $+WRMS$  at the end of the total observation period  $T$ , respectively, i.e., by  $2WRMS/T$  where the WRMS represents the actual scatter in each time series. This straightforward approach works very well for stations observed more than twice, and does not require the use of an empirical error model [Mao *et al.*, 1999] tuned by different types of site-specific noise behavior [Dixon *et al.*, 2000; Williams *et al.*, 2004]. Although it is not directly evident from the theory, this noise error model is also strongly correlated to the WRMS, and can be rewritten as  $2WRMS/T$  multiplied by a “noise correction coefficient,” which was found to typically vary between 0.5 and 1.5.

[17] Byproducts of the geodetic results are the improved and more accurate velocity estimates in ITRF2000 for IGS stations BAKO, NTUS, and PIMO. The SEAMERGES velocity field, which is based on long time series, will provide important information to aftermath studies of the rare great 2004 Sumatra-Andaman earthquake because accurate interseismic velocities enable better estimation of both size and duration of postseismic deformations. These could be due to poroelastic rebound and viscoelastic relaxation [e.g., Pollitz and Dixon, 1998].

## 4. Sundaland Boundaries, Motion, and Deformation

### 4.1. Block Definition

[18] Details of the deformation in and near the Sundaland block are embedded in the GPS velocity field. To define these deforming regions, (internal) strain rates are estimated in polygons using the approach described by Feigl *et al.*

[190]. The intraplate and interplate deformation in SE Asia is shown in the left and right panels of Figure 3, Figure 4 respectively. From the analysis of the strain-rate tensors, it is possible to localize a zone of very low strain rate, below  $7 \times 10^{-9} \text{ yr}^{-1}$ , which represents the undeformed interior of the Sundaland block. The term block instead of plate is used because the region's nonhomogeneous history disfavors quasi-rigid behavior on a geologic timescale [Hall and Morley, 2004]. The name Sundaland is used because this biogeographical region makes up the largest (visible) part of the block. Its core (khaki-green area in Figure 3) geographically covers Vietnam, Laos, Cambodia, Thailand, Peninsular Malaysia, the Sunda shelf, Borneo, and parts of Sumatra and Java. Most of the Sundaland block boundaries have been previously identified or suggested [e.g., Chamote-Rooke and Pichon, 1999; Rangin et al., 1999; Simons et al., 1999; Kreemer et al., 2000; Michel et al., 2001; Bock et al., 2003], as they correspond to well known active fault zones. These boundaries are refined and summarized below in a consistent overview.

[19] To the west, the Sundaland block is bounded by a right lateral shear zone that is clearly defined by the strain tensor principal directions (Figure 3). It extends from Myanmar to Sumatra along the Sagaing Fault [Tapponnier and Molnar, 1975; Le Dain et al., 1984; Peltzer and Saucier, 1996], the Andaman pull-apart system [Curry et al., 1979; Weissel, 1981], and the Great Sumatran fault [Fitch, 1972; McCaffrey, 1991; Bellier and Seberier, 1995].

[20] To the south of Java, the block is enclosed by the Java trench [Hamilton, 1979; Kappel, 1980; McCaffrey, 1991]. However, the island of Java is affected by significant deformation (Figure 3). The deformation corresponds to left-lateral strike-slip faulting on central Java and is associated with inland seismicity [Newcomb and McCann, 1987], most recently testified by the 2006 Yogyakarta earthquake [Earthquake Engineering Research Institute, 2006]. If this active faulting is confirmed, only the western part of Java is part of Sundaland and a (segmented) strike-slip fault (oriented northeastward) outlines the southern boundary of the block east of  $110^\circ\text{E}$ .

[21] To the east, considerable deformation affects Sulawesi (eastern Indonesia) and only the southwestern part was considered to be part of the Sundaland (or Sunda Shelf) block [Walpersdorf et al., 1998; Stevens et al., 1999; Simons et al., 1999; Bock et al., 2003]. However, the high strain rates (Figure 3) between Borneo and Sulawesi (dense GPS subset available) show that the entire island is not part of the Sundaland block [Socquet et al., 2006a]. Deformation continues until the eastern margin of Borneo through the Makassar Strait which gives shape to its eastern boundary between  $-10^\circ\text{N}$  and  $5^\circ\text{N}$ . North of Sulawesi, the Philippine belt [Rangin, 1991; Rangin et al., 1999] skirts Sundaland. This region is affected by very high strain rates (Figure 3), and the eastern boundary of the Sundaland block is here considered [Rangin et al., 1999] to follow the three trenches west of the Philippine islands: the Cotabato, Negros, and Manilla Troughs (Figure 1).

[22] To the north, the Sundaland boundaries can not be defined from the strain rate analysis. The South China Sea appears undeformed and the South China block (pink area in Figure 3) [Gordon, 1995; Calais et al., 2003; Shen et al., 2005] shows only low strain rates. Although the South

China block [Shen et al., 2005] (Figure 1) shows no signs of internal deformation, it is bounded to the west by the Longmenshan and Xiaojiang faults. Beyond these faults lies an actively deforming region where, driven by the India-Eurasia continental collision, crustal material is transported down from the Tibetan plateau in a clockwise deformation pattern around the Eastern Himalayan Syntaxis (EHS) [Holt et al., 1991; Wang et al., 1998; Iwakuni et al., 2004; Shen et al., 2005]. This deformation extends into Myanmar and appears to affect the north of Thailand by east-west extension. The increased strain rates in northwest Thailand (Figure 3) confirm Sundaland's northern boundary lies nearby in Myanmar. To the northeast, the southeastern part of the Red River fault [Tapponnier and Molnar, 1977; Allen et al., 1984; Leloup et al., 1995] draws a geological boundary between the Sundaland and South China blocks. The strain tensors (Figure 3) are here compatible with right-lateral shear, but any deformation across this boundary appears small at the present time [Weldon et al., 1994; Wang et al., 1998; Feigl et al., 2003]. At this point, using only the strain analysis from the "large-scale" network makes it difficult to conclude if South China and Sundaland have different eastward motions or not.

#### 4.2. Rotation Vector Estimation

[23] The strain rate analysis locates  $\sim 40$  velocity vectors on (undeformed) Sundaland that can be inverted to extract an angular velocity vector of a single tectonic entity [DeMets et al., 1994]. Because the velocity field is not uniform in terms of precision or distribution, an equally weighted and equally spaced subset was first selected to estimate the rotation pole, thereby excluding the deforming boundaries (Figure 3). The misfit criterion to accept/reject sites is 3 mm/yr and results from a tradeoff between (relative) accuracy, unbalance in the network, data impact factors and possible deformation noise. The final estimate of the Sundaland block rotation pole and rate (Table 2) uses 28 sites, the RMS residual velocity is 1.8 mm/yr and 75% of the selected sites have residual velocities smaller than 2 mm/yr (see Figures 3 and 5) Also PHUK, ARAU, USMP, BEHR, and SEGA met the criterion, but were excluded because small but systematic (1–3 mm/yr) residuals on the Malay Peninsula are more pronounced here. Such details of intraplate deformation are also visible in N Borneo (Sabah) [Rangin et al., 1999] and NW Thailand (Chiang Mai) [Iwakuni et al., 2004; Fenton et al., 2003; Rhodes et al., 2004] and attest to the remarkable level of resolution obtained by the data analysis. The larger residuals observed in Sundaland's boundary zones (shown in Figure 6 for Myanmar, Sumatra, Java, Bali, and across the Makassar Strait) are unmistakably related to inter-plate deformations. Altogether, the rotation vector represents the most reliable estimate of Sundaland's motion before the Mw 9.2 earthquake of December 2004. Figure 6 shows the velocity residuals of all sites in the region with respect to this result.

#### 4.3. Comparison With Previous Estimates

[24] Comparison with (absolute) rotation vectors published by previous studies (Table 2) has revealed significant shortcomings in these results. Although they detected the motion of Sundaland with respect to Eurasia, the first two GEODYSSSEA results [Wilson et al., 1998; Simons et al.,

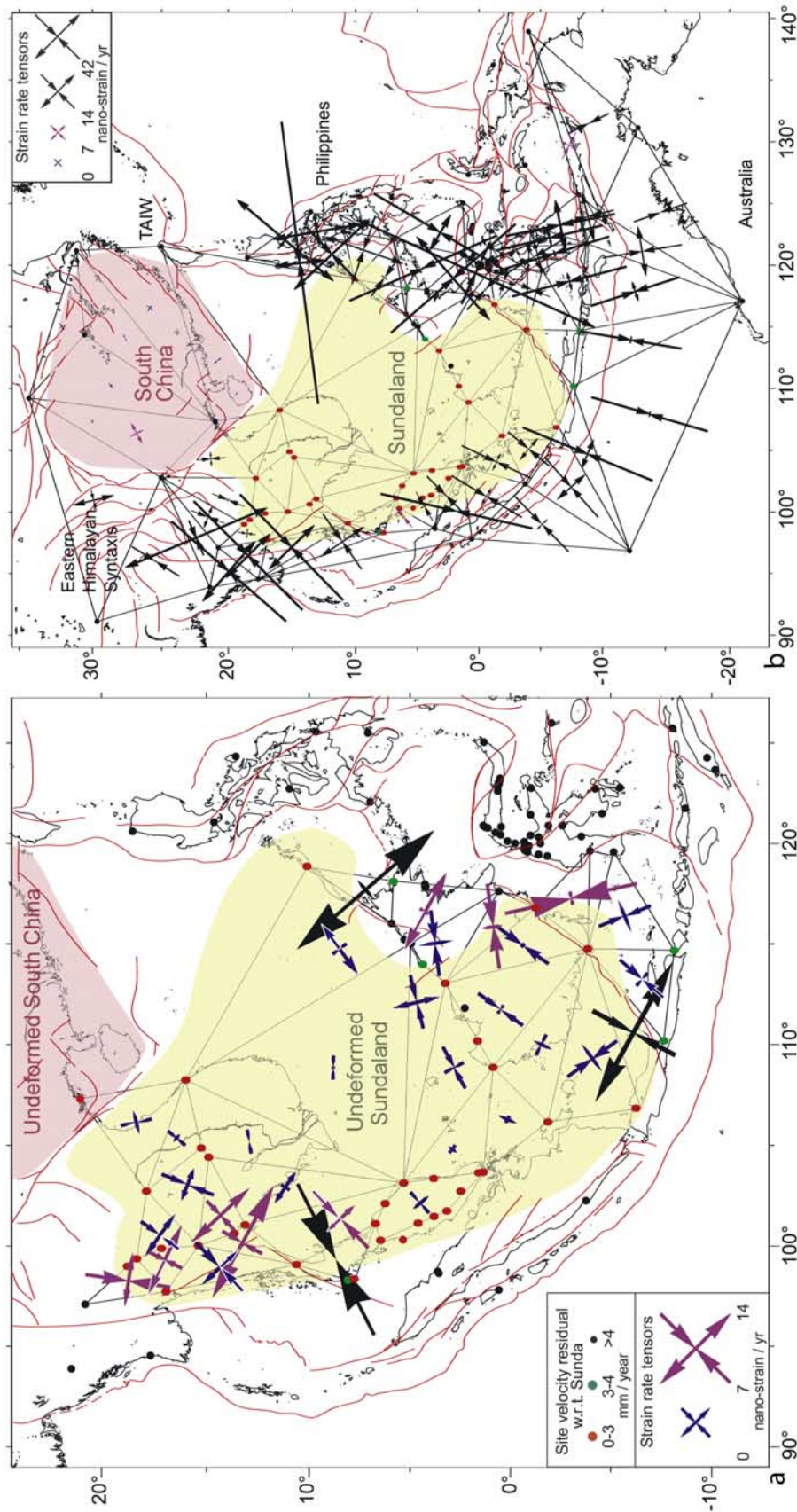


**Figure 3.** Deformation in and around Sundaland block, showing the deformation (a) inside and (b) outside Sundaland, respectively. The strain rate tensors (scaled in nanostrain/yr) have been computed from the velocity solution presented in this paper, except for station TAIW whose velocity was taken from the TNML time series by JPL in ITRF2000 (<http://sideshow.jpl.nasa.gov/mbh/series.html>). Main active faults are shown in red. The colored dots localize the GPS stations processed in this solution. Red dots represent stations with a residual velocity with respect to Sundaland below 3 mm/year, green ones between 3 and 4 mm/yr, and black ones above 4 mm/yr.

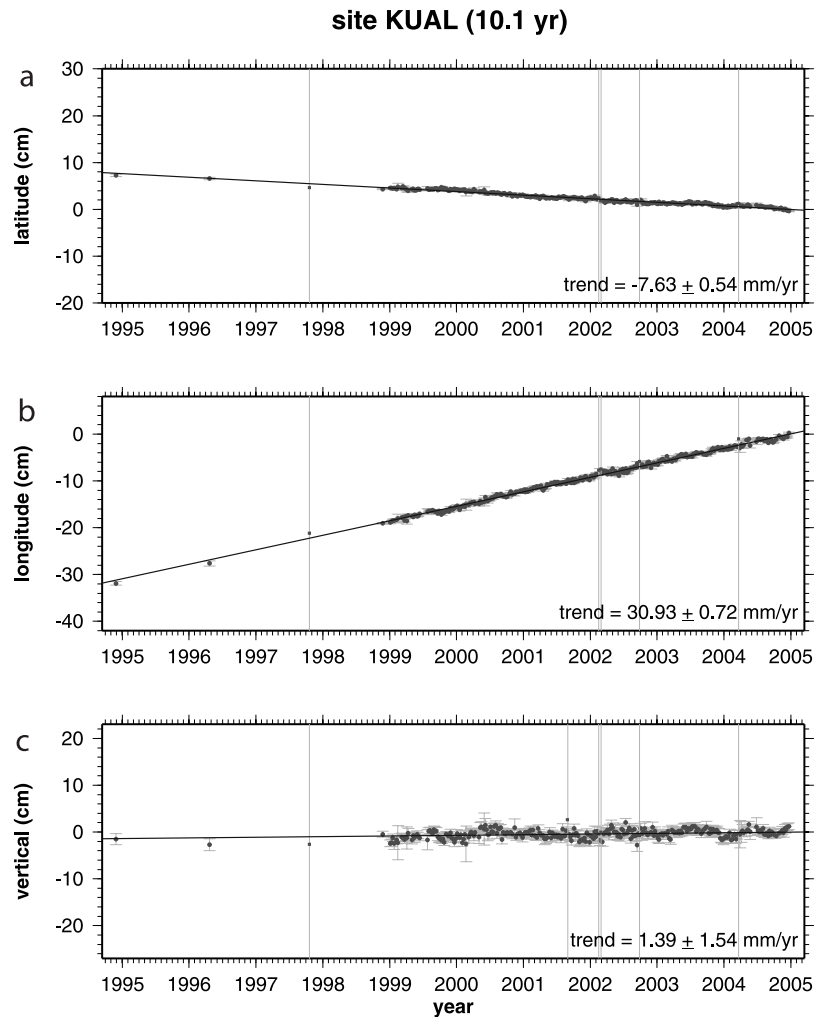


**Figure 4.** Coordinate time series station KUAL in ITRF2000. This Malaysian GPS station originally was a GEODYSSSEA site and became a permanent MASS station at the end of 1998. The total time span used to compute the (ITRF2000) velocity estimate is 10.1 years. The figure shows five automatically marked three-dimensional (3-D) outliers in 1997, 2002, and 2004 and 1 vertical-only outlier in 2001 (with misfits above 8, 11, and/or 25 mm in north, east, and up, respectively) while the other weekly averaged positions line up nicely. Up to 6 years of permanent GPS data were analyzed for the Malay MASS GPS network. The uncertainties of the velocity components are at the 95% confidence level. Time series for the analyzed SE Asia + IGS network can be downloaded from <http://www.deos.tudelft.nl/~wims/sunda.html>.

1999] were inaccurate because of poorly defined reference frames. Even with improved mapping accuracy, *Michel et al.* [2000] did not have the resolution to distinguish between South China and Sundaland motion. The final consensus solution [*Michel et al.*, 2001] abandoned this single block idea and used 10 sites on Sundaland (in Figure 6: NONN, CHON, PHUK, KUAL, TABA, TANJ, BATU, BAKO, BATU, and BALI). Furthermore, in the work of *Michel et al.* [2001], Sundaland's (larger) relative motion was referenced using the Nuvel-1A NNR pole for Eurasia [*DeMets et al.*, 1994], instead of ITRF [*Altamimi et al.*, 2002].

[25] The REVEL plate model of *Sella et al.* [2002] considered a Sundaland plate using ITRF97 velocities of three IGS stations (BAKO, NTUS, KUNM), but the Kunming station in China (large residual in Figure 6) lies in the actively deforming region around the EHS [*Wang et al.*,

1998; *Shen et al.*, 2005]. Therefore the reported Sundaland pole location and rate are poorly constrained by only two velocity estimates (as repeated in ITRF2000 by *Prawirodirdjo and Bock* [2004]).

[26] The *Kreemer et al.* [2003] study on a global plate No-Net-Rotation (NNR) model used the GPS velocities of *Michel et al.* [2001] and added IGS station NTUS. Their rotation vector for Sundaland predicts motions similar to *Michel et al.* [2001] across Sundaland, indicating their own NNR conditioned reference frame is aligned with ITRF2000 in the SE Asia region.

[27] The most recent paper by *Bock et al.* [2003] extensively discusses crustal motion in Indonesia. A Sunda Shelf block is defined with a boundary along the Palu-Koro fault and therefore includes South Sulawesi [*Socquet et al.*, 2006a], Taiwan, and presumably encompassing at least South China below the IGS sites SHAO, WUHN, and

**Table 2.** Absolute and Relative Rotation Vectors for the Sundaland, Eurasian, South China, and Australian Plates<sup>a</sup>

Reference	Reference Frame	Sites Used	Pole Rotation Parameters			Uncertainties			
			Lat, °N	Lon, °E	$\omega^\circ/\text{Myr}$	$\sigma_{\text{maj/lat}}^\circ$	$\sigma_{\text{min/lon}}^\circ$	Azimuth <sup>o</sup>	$\chi^2$
<i>Absolute Rotation Vectors</i>									
Sundaland Block									
GEODYSSSEA									
<i>Wilson et al.</i> [1998]	ITRF94	12	31.8	−46	0.28	-	-	-	-
<i>Simons et al.</i> [1999]	ITRF96	12	51	−113	0.23	-	-	-	-
<i>Michel et al.</i> [2000] <sup>b</sup>	ITRF97	15	59.7	−102.7	0.34 ± 0.01	2.9	3.9	NA	-
<i>Michel et al.</i> [2001]	ITRF97	10	56.0	−102.7	0.339 ± 0.007	-	-	-	-
<b>This study</b>	<b>ITRF00</b>	<b>28</b>	<b>49.0</b>	<b>−94.2</b>	<b>0.336 ± 0.007</b>	<b>1.9</b>	<b>0.3</b>	<b>111</b>	<b>1.03</b>
Others									
<i>Sella et al.</i> [2002]	ITRF97	2	38.9	−86.9	0.393 ± 0.062	10.2	0.8	110	0.24
<i>Kreemer et al.</i> [2003]	NNR	9	47.3	−90.2	0.392 ± 0.008	1.9	0.5	109	3.11
<i>Bock et al.</i> [2003] <sup>b</sup>	ITRF00	16	49.8	−95.9	0.320 ± 0.010	3.5	1.0	121	1.20
<i>Prawiro et al.</i> [2004]	ITRF00	2	32.6	−86.8	0.462 ± 0.064	7.0	0.8	113	4.00
Eurasian Plate									
<i>Bock et al.</i> [2003]	ITRF00	18	58.3	−97.2	0.260 ± 0.001	1.5	0.3	48	1.80
<i>Prawiro et al.</i> [2004]	ITRF00	18	57.2	−99.7	0.260 ± 0.002	0.8	0.2	52	1.10
<i>Altamimi et al.</i> [2002]	ITRF00	19	58.0	−99.4	0.260 ± 0.005	1.2	2.7	NA	-
<i>Shen et al.</i> [2004] <sup>c</sup>	ITRF00	11	55.6	−102.4	0.252 ± 0.010	1.8	0.9	56	-
<i>Fernandes et al.</i> [2003]	ITRF00	58	54.6	−103.9	0.249 ± 0.003	1.6	0.4	51	-
<b>Calais et al.</b> [2003]	<b>ITRF00</b>	<b>15</b>	<b>52.3</b>	<b>−107.0</b>	<b>0.245 ± 0.005</b>	<b>0.2</b>	<b>0.2</b>	<b>NA</b>	<b>-</b>
<i>Demets et al.</i> [1994]	NUVEL-1A		50.6	−112.3	0.234	-	-	-	-
South China Block									
<b>Shen et al.</b> [2004] <sup>c</sup>	<b>ITRF00</b>	<b>81</b>	<b>61.2</b>	<b>−115.6</b>	<b>0.322 ± 0.002</b>	<b>1.4</b>	<b>0.1</b>	<b>134</b>	<b>1.04</b>
Australian Plate									
<i>Altamimi et al.</i> [2002]	ITRF00	4	32.3	39.4	0.614 ± 0.006	0.7	0.8	NA	-
<i>Beavan et al.</i> [2002]	ITRF00	11	32.8	37.5	0.621 ± 0.002	0.4	0.1	161	1.08
<i>Fernandes et al.</i> [2003]	ITRF00	11	32.4	38.8	0.621 ± 0.005	1.5	0.5	151	-
<i>Wallace et al.</i> [2004]	ITRF00	11	32.0	39.1	0.621 ± 0.003	0.6	0.3	163	-
<b>This study</b>	<b>ITRF00</b>	<b>6</b>	<b>32.9</b>	<b>38.1</b>	<b>0.621 ± 0.004</b>	<b>0.9</b>	<b>0.3</b>	<b>151</b>	<b>1.01</b>
<i>Relative Rotation Vectors</i>									
Sundaland/Eurasia									
<b>This study</b>	<i>Calais et al.</i> [2003]	28/15 <sup>d</sup>	<b>36.2</b>	<b>−70.0</b>	<b>0.101 ± 0.010</b>	<b>5.8</b>	<b>2.2</b>	<b>78</b>	<b>1.02</b>
Sundaland/Australia									
<b>This study</b>	<b>This study</b>	28/6 <sup>d</sup>	<b>−6.9</b>	<b>−128.2</b>	<b>0.694 ± 0.009</b>	<b>1.2</b>	<b>0.5</b>	<b>14</b>	<b>1.03</b>
South China/Eurasia									
<i>Calais et al.</i> [2003]	<i>Calais et al.</i> [2003]	9/15 <sup>c</sup>	60.6	136.7	0.123 ± 0.012	4.6	1.1	NA	-
<i>Shen et al.</i> [2004]	<i>Shen et al.</i> [2004]	81/11 <sup>d</sup>	63.7	182.0	0.083 ± 0.005	4.5	0.5	7	1.04
<b>Shen et al.</b> [2004]	<i>Calais et al.</i> [2003]	81/15 <sup>d</sup>	<b>75.2</b>	<b>173.1</b>	<b>0.091 ± 0.006</b>	<b>4.1</b>	<b>2.7</b>	<b>32</b>	<b>1.03</b>
Sundaland/South China									
<b>This study</b>	<i>Shen et al.</i> [2004]	28/81 <sup>d</sup>	<b>−17.1</b>	<b>−57.2</b>	<b>0.099 ± 0.015</b>	<b>2.9</b>	<b>1.7</b>	<b>153</b>	<b>1.03</b>

<sup>a</sup>NA: Not applicable. References in boldface are the ones computed and/or used in this paper. Previous estimates are listed for comparison. Here  $\omega$  is positive for counterclockwise (CCW) rotation,  $\sigma_{\text{maj/lat}}$  and  $\sigma_{\text{min/lon}}$  are the semimajor and semiminor axes of the 1- $\sigma$  pole error ellipse or the latitudinal and longitudinal 1- $\sigma$  uncertainties of the pole position. The azimuth of the major error ellipse axis is given CCW from the east. The reduced  $\chi^2$  is defined as the sum of squared weighted residuals divided by the degrees of freedom.

<sup>b</sup>Describe Sundaland and South China as a single block at the 3–5 mm/yr level.

<sup>c</sup>Provided by *Shen et al.* [2004]. The South China block rotation vector in ITRF2000 is wrongly printed in the work of *Shen et al.* [2004].

<sup>d</sup>(Re)computed by combining rotation vectors derived relative to ITRF2000. Given as rotation of the first-referenced plate relative to the second. For Sundaland/Australia one single ITRF2000 velocity field was used. For Sundaland/South China overlapping stations in both velocity fields were used to verify the independent realizations in ITRF2000.

<sup>e</sup>Describes north and south China as a single block at the 2 mm/yr level.

XIAN similar to *Michel et al.* [2000]. The solution presented in the paper of *Bock et al.* [2003] is a bit of a mystery. Their Sunda Shelf rotation vector matches quite well with the solution presented in this paper, but the data they used does not support their result. When the same inversion was attempted, only three of the 16 velocity vectors appear to control the estimation of the rotation pole position and rate. The uncertainty of the other vectors is so large that they hardly contribute to the estimation. All vectors fit with a 2-D RMS of 7.1 mm/yr (compared to 1.8 mm/yr for 28 sites in Figure 5), which is too low to obtain a reliable estimate. The solution appears to be

dominated by the velocity vectors of only three stations (which have 75% of the data weighting assigned), one of which (BAKO) is deeply south in the network (and potentially perturbed by local deformation) and the other two SHAO and WUHN are far to the north in China, which is not part of the Sundaland block as shown in the next section. The residuals of all 16 velocity vectors of *Bock et al.* [2003] with respect to Sundaland are presented in the electronic supplement. Taking into account the limited accuracy of most velocity vectors, they primarily express local deformation in Indonesia, as presented for example by *Tregoning et al.* [1994] and *Genrich et al.* [1996]. Only the

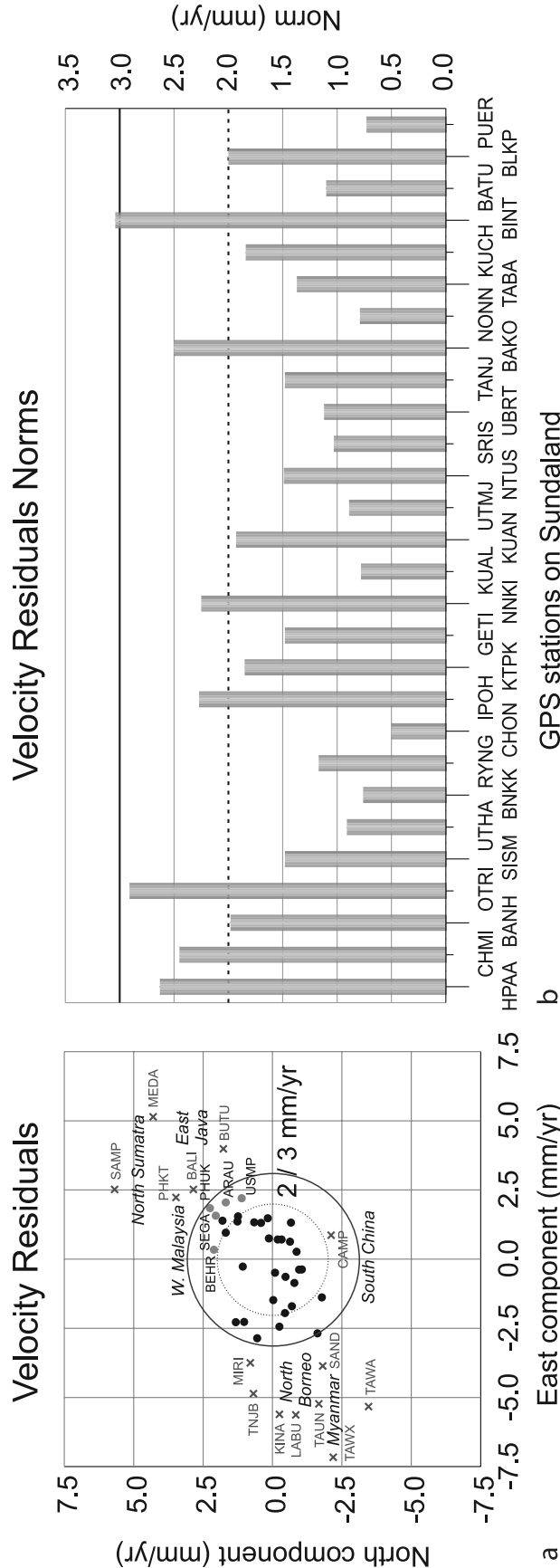


**Figure 5.** Residual vectors of stations on Sundaland showing (a) north and east components of the residual vectors for the 28 sites located on undeformed Sundaland (black dots) and 14 sites located in the Sundaland boundary deformation zones (gray crosses). The residuals have the same characteristics in each of these named zones. The circle with 3 mm/yr radius represents the misfit criterion to accept/reject sites on Sundaland. Five stations within the criterion radius (gray dots) were excluded because they are affected by accumulated elastic deformation from the plate convergence at the Sumatra trench. Also shown are (b) norms of the residual vectors for the 28 stations on Sundaland, sorted according to their longitude from HPAA in South Myanmar to PUER on Palawan Island in the Philippines. The RMS of all residual norms is 1.8 mm/yr whereby 75% of the norms are smaller than 2 mm/yr.

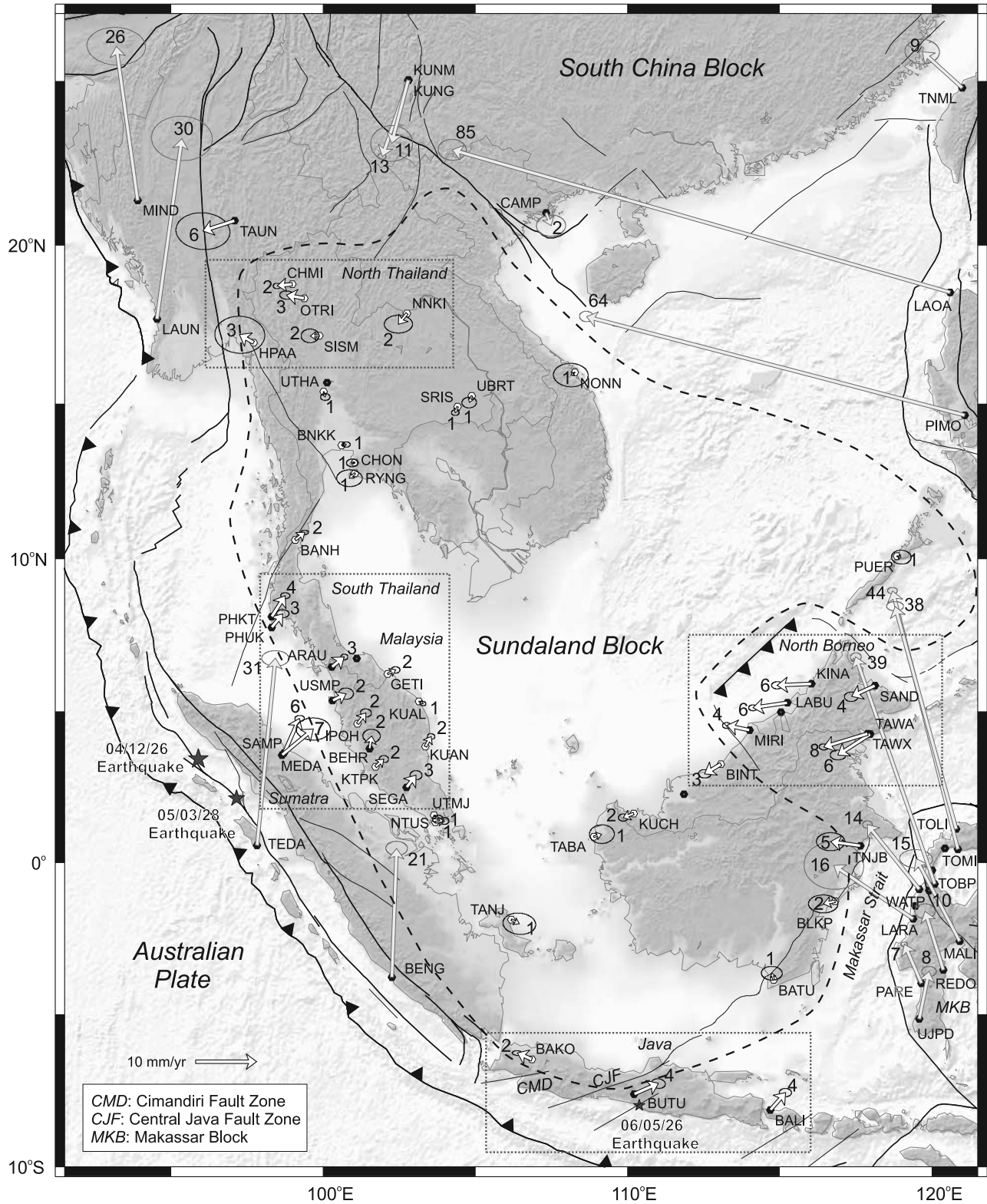


Figure 6

motion of station DEMU on Sumatra is consistent with the results of strain accumulation in this region (Figure 6). For the rest, the apparent correctness of the *Bock et al.* [2003] rotation vector for Sundaland seems to be a coincidence.

[28] Although the absolute rotation vector of Sundaland in ITRF97 given by *Michel et al.* [2001] was not significantly and reliably improved until now, the existence of an independently moving Sundaland block is commonly accepted. However, the relative motion with respect to Eurasia is still poorly constrained; the absolute pole locations of Sundaland and Eurasia are close to each other and the results for the absolute motion of Eurasia in ITRF2000 [e.g., *Altamimi et al.*, 2002; *Bock et al.*, 2003; *Prawirodirdjo and Bock*, 2004; *Fernandes et al.*, 2003; *Calais et al.*, 2003] (Table 2) are still diverging.

#### 4.4. Relative Motion and Plate Boundary Deformation

[29] The relative motion of Sundaland with respect to the Indian (IN) plate and the Sundaland/Australia/Philippine triple plate junction is extensively discussed in two previous companion papers [*Socquet et al.*, 2006a, 2006b] that both make partial use of the SE Asia velocity field presented here. Only the deformation inside Sundaland across these plate boundaries is discussed below. Around the Sundaland block, these interplate deformation rates can reach very high values (Figure 3b) due to the high relative plate motions here. It is possible to see a progressive increase in the deformation rate from the core of Sundaland to its boundaries (Figure 3a). These zones of intermediate deformation rate surrounding the rigid core indicate that high-rate interplate deformation takes place at wide boundaries and remains detectable up to 750 km inside Sundaland. The SE Asia network presented here was not extensive enough to infer any new results on the geodynamic behavior with respect to the Philippine (PH) plate boundary.

##### 4.4.1. Sundaland/Eurasia

[30] The GEODYSSSEA project [*Michel et al.*, 2001] reported two possible interpretations for the identified motion of Sundaland with respect to Eurasia (as defined in NNR-NUVEL-1A by *DeMets et al.* [1994]): “Either the motion is eastward at an average rate of  $12 \pm 3$  mm/yr or the block also rotates clockwise with respect to Eurasia at a velocity increasing from 10 mm/yr in the south to 14 mm/yr in the north. The use of ITRF97-velocities for the definition of Eurasia as a reference diminishes the escape velocity to 8 mm/yr.” The solution presented here confirms the second description with Sundaland rotating clockwise with respect to (NNR-NUVEL-1A) Eurasia at velocities of 7 to 11 mm/yr

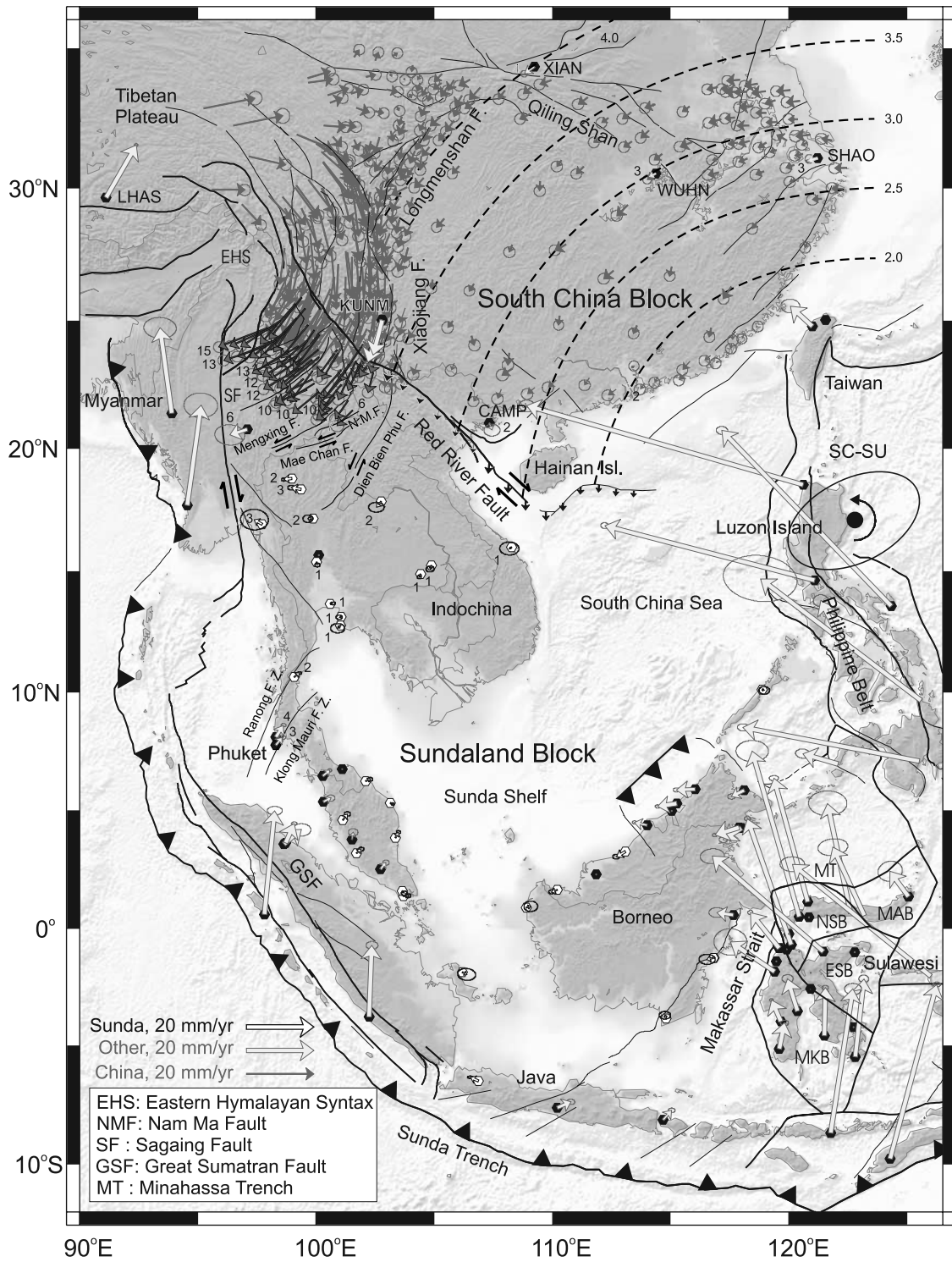
from south to north, respectively. The decrease by  $\sim 3$  mm/yr compared to *Michel et al.* [2001] mainly results from the differences between ITRF2000 and ITRF97.

[31] The absolute rotation vectors of NNR-NUVEL-1A are not identical to those estimated in the ITRF2000 [*Altamimi et al.*, 2002]. In fact, many different Eurasia plate motion models have been derived [e.g., *Sella et al.*, 2002; *Bock et al.*, 2003; *Fernandes et al.*, 2003; *Nocquet and Calais*, 2003; *Steblov et al.*, 2003; *Calais et al.*, 2003; *Prawirodirdjo and Bock*, 2004]. Unfortunately, they all have a bias toward Western Europe where  $\sim 90\%$  of the available GPS stations cover only a tiny part of the plate. Here the models agree within  $\pm 1$  mm/yr, but farther east the differences become larger. For example, in East Asia the relative motion predictions at Shanghai can vary up to 4 mm/yr in SW-NE direction. Therefore at present the best compromise is the Eurasia model (Table 2) of *Calais et al.* [2003] because it includes more GPS data from Siberia. The motion of Sundaland (SU) with respect to Eurasia (EU), described by the relative SU-EU vector in Table 2, is 6 mm/yr oriented (azimuth from North)  $N85^\circ$  north of Java, increasing to 9 mm/yr oriented  $N80^\circ$  in Indochina. This result is more consistent, and although smaller than with respect to NNR-NUVEL-1A, it still indicates a clockwise rotation of Sundaland with respect to the European-Siberian core of the Eurasian plate. Interestingly, the Eurasia vectors from ITRF2000 [*Nocquet and Calais*, 2003; *Fernandes et al.*, 2003; *Steblov et al.*, 2003; *Calais et al.*, 2003] appear to converge toward the NNR-NUVEL-1A model (Table 2).

##### 4.4.2. Sundaland/South China

[32] Previous regional GPS studies considered the relative motion between South China (SC) and Sundaland to be zero [e.g., *Michel et al.*, 2000; *Bock et al.*, 2003; *Iwakuni et al.*, 2004] or small ( $< 5$  mm/yr) [e.g., *Michel et al.* 2001]. Local GPS studies in China and Vietnam across the central and southern segments of the Red River fault (RRF) (east of  $101^\circ E$  in Figure 6) [*King et al.*, 1997; *Chen et al.*, 2000; *Feigl et al.*, 2003; *Shen et al.*, 2005] estimated right-lateral strike-slip rates at 0–3 mm/yr, consistent with the result of a fault-trenching study by *Weldon et al.* [1994]. So any relative motion is indeed small, but not necessarily zero if (partially) accommodated by the RRF. With respect to the refined Sundaland motion, the three IGS subset stations in South China (WUHN, SHAO, XIAN) clearly move 2–4 mm/yr WSW (Figure 7). Their motions of  $\sim 8$  mm/yr ESE with respect to Eurasia fit better to a counterclockwise rotating SC block at 7–8 mm/yr ESE [*Shen et al.*, 2000; *Wang et al.*, 2001], or a counterclockwise rotating single

**Figure 6.** SEAMERGES GPS velocities with regard to Sundaland. White arrows with open dots (28) represent the station velocities (uncertainties at 95% confidence level) used to compute the motion of the undeformed core of the Sundaland block (approximately encompassed by the dashed curve). White arrows with solid dots (18) represent stations in the deformation zones. For clarity not all available vectors on Sulawesi are plotted (black dots). Velocities of four sites on Sundaland with high uncertainties were excluded from the GPS results (black dots in Thailand, Malaysia, and Brunei). Some stations have two vectors representing independent solutions of the same point due to station relocation or because adjacent points overlap. The similarity of these vectors also provides a good indication of the quality of the solution. The integer numbers near the vector heads are the norm of the velocity vector in mm/yr. Thick and thin solid black lines depict the primary and secondary fault systems in the region, and the annotated lines represents the trace of the trenches associated with active subduction. The boxes denote the four investigated Sundaland boundary zones that exhibit clear deformation patterns. The star symbols denotes the locations of the nucleation events that triggered the Mw 9.2 (Banda-Aceh), 8.7 (Nias), and 6.3 (Central Java) earthquakes. Note the magnitude and direction of the vectors of the stations Medan (MEDA) and Sampali (SAMP) in northern Sumatra, which provide a clear indication of coupling before the earthquake.



North and South China block at 7–11 mm/yr ESE [*Calais et al.*, 2003].

[33] The SC block was unambiguously defined (86 sites) by *Shen et al.* [2005] and used as a stable reference to study crustal deformation in southwest China. The relative SC-EU vector of *Shen et al.* [2005] was reproduced from the available velocity field and slightly refined with a 2.5 mm/yr outlier criterion. The matching SC and EU vectors in ITRF2000 were kindly provided by the authors of *Shen et al.* [2005] (Table 2). With the velocity solution of *Shen et al.* [2005] the relative SU-SC vector could be estimated (Table 2). Only small scattered differences ( $<0.6$  mm/yr) exist between the velocity components of sites available in both GPS solutions (WUHN, SHAO, KUNM in Figure 7).

[34] Relative to Sundaland, South China rotates counterclockwise around a pole east of Luzon (Phillipines) at 1–4 mm/yr in WSW to SSW directions (Figure 7). This implies shortening along the boundary between SU and SC with mainly a N-S component that increases to the west away from the rotation pole. With respect to Eurasia (as defined by *Calais et al.* [2003]) South China moves at 8 mm/yr oriented  $N105^\circ$  in Shanghai to 9 mm/yr oriented  $N105^\circ$  near the Red River fault, where Sundaland moves at 9.5 mm/yr oriented  $N85^\circ$ . The differential motion along the fault (SE of  $23^\circ N$   $103^\circ E$  in Figure 7) indicates a maximum possible right-lateral strike-slip rate of  $1.6 \pm 0.5$  mm/yr with a compression component of  $2.8 \pm 0.4$  mm/yr that decreases to the east. This agrees with the relative motion of CAMP in Figure 7, which predicts a slip rate of 2 mm/yr. Unfortunately, no velocity vectors are available directly to the south of the RRF.

[35] Therefore any deformation along this part of the Red River fault is smaller than the up to 5 mm/yr slip estimates predicted from neotectonic studies [*Allen et al.*, 1984; *Leloup et al.*, 1995; *Replumaz et al.*, 2001]. The latest results are compatible with local geodetic evidence [*King et al.*, 1997; *Chen et al.*, 2000; *Feigl et al.*, 2003; *Shen et al.*, 2005] on the RRF, but contrary to *Michel et al.* [2000], *Bock et al.* [2003], and *Iwakuni et al.* [2004], clearly show the existence of a relative motion between SU and SC that needs to be accommodated along their common boundaries. This implies low deformation rates ( $<1$  mm/yr) east of Hainan Island ( $19^\circ N$   $110^\circ E$ ) due to the short distance to the SC-SU rotation pole (Table 2) located east of Luzon in Figure 7. Here the RRF ends in the South China Sea Basin, characterized by a very slow and further decreasing strain

rate (Figure 3) in the South China Sea. Therefore the South China Sea can be considered here as a diffuse boundary zone (between SU, SC, and PH) where the Red River fault no longer has a clear surface expression.

[36] The combined velocity field gives a better insight into the deformation zone that lies in between South China/Sundaland and the Eastern Himalayan Syntaxis (Figure 7). As in southwest China, the observed clockwise deformation pattern results in left-lateral shear at the northwest boundary of the undeformed Sundaland block. In contrast to the South China block where this shear zone is bounded by the Xianshuihe-Xiaojiang fault, deformation to the southwest of the Red River fault is accommodated by multiple NE-SW strike-slip faults [*Lacassin et al.*, 1998; *Shen et al.*, 2005] that do not appear to reach the Sagaing fault in Myanmar. The Mengxing fault (China), the Mae Chan fault (Thailand and Laos), and the north segment of the Dien Bien Phu fault (Laos and Vietnam) make up the northwest boundary of the undeformed Sundaland block (Figure 7). The estimates of the maximal strike-slip motion on these faults ( $\sim 4 \pm 2$  mm/yr) are in approximate agreement with the results based on river offsets by *Lacassin et al.* [1998]. Interestingly, seismic activity in the southern part of the shear zone diminishes in SW direction and strike-slip faults extend less further to the west in SE direction. This favors the proposed refined models [e.g., *Shen et al.*, 2005; *Schoenbohm et al.*, 2006] describing present motion around the EHS as the detached flow of the upper crust from the uplifted Tibetan plateau to the southeast due to gravitational buoyancy forces associated with the sharp topographic gradient across the region, but disfavors the suggested role of trench-roll back in Myanmar since no extension inside the shear zone is observed. Instead the crustal flow is diverted southward by the South China block, southwestward by the Sundaland block and accumulates east of the Sagaing fault in Myanmar.

#### 4.4.3. Sundaland/Australia

[37] The rotation vector for Australia was computed by minimizing the GPS velocities of 6 stations on the Australian (AU) plate (DARW, KARR, YAR1, PERT, TIDB, COCO) available from the analysis in this paper (Table 2). The residual velocities are all below 2 mm/yr except for COCO where a seismic jump was estimated in 2000. The absolute AU vector matches very well with other results in ITRF2000 [*Altamimi et al.*, 2002; *Beavan et al.*, 2002; *Fernandes et al.*, 2003; *Wallace et al.*, 2004] and the predicted motions along the boundaries with SE Asia all agreed within 1 mm/yr. Combined with the defined vector for

**Figure 7.** Velocities in SE Asia with respect to Sundaland. The South China velocity field of *Shen et al.* [2005] (with black outlines SW of the Red River Fault (RRF)) was successfully aligned and verified with 3 overlapping IGS stations (WUHN, SHAO, and KUNM). The relative South China/Sundaland rotation pole (with  $1-\sigma$  uncertainties) is located east of Luzon Island, along with the predicted (counterclockwise) relative velocities (black arrows) along the southern segment of the RRF. Dashed circular arcs represent predicted South China tangent velocities of 2.0, 2.5, 3.0, 3.5, and 4.0 mm/yr, respectively. The upper crustal flow around the EHS generates left-lateral shear on the Sundaland block in Southwest China, East Myanmar, North Laos, and North Thailand. The accommodating left-lateral strike-slip faults' naming convention and traces are based on *Lacassin et al.* [1998], *Fenton et al.* [2003], *Shen et al.* [2005], and satellite images accessible through Google<sup>TM</sup> Earth. The relative motion of Phuket Island is caused by elastic strain accumulation from the shallow subduction process at the Sumatra trench possibly combined with motion on the active Ranong and/or Klong Mauri faults (identified by *Fenton et al.* [2003]). The micro-blocks making up Sulawesi [*Socquet et al.*, 2006a] were also resolved using the GPS data analysis results (MAB: Manada Block, NSB: North Sula Block, ESB: East Sula Block, and MKB: Makassar Block).

Sundaland in ITRF2000, the relative motion of Australia and Sundaland is obtained (Table 2). Near the IN/AU/SU triple plate junction at the intersection between the Andaman and Sumatra sections of the Sunda Trench and the 90° E Ridge (9°N) the predicted relative motion is 47 mm/yr (oriented) N0° and southward increasingly becomes less oblique to the trench along Sumatra at 55 mm/yr N10° at the equator near Nias Island to 63 mm/yr N14° south of the Sunda Strait. To the north of Sumatra, the Indian plate subducts along the trench below the Andaman Islands and Myanmar [Socquet *et al.*, 2006b].

[38] South of Java island the motion becomes perpendicular to the trench at 67 mm/yr N14° and again slightly oblique at 70 mm/yr N13° to the south of Bali. The convergence of Australia and Sundaland is marked by the curving Sunda (Sumatra/Java) Trench subduction zone. Here the main compressive strain axis remains normal to the subduction axis (Figure 3), and hence rotates slightly clockwise from NNW-trending to the east (south of Sulawesi and Flores islands) to NE-trending to the west (in the Sumatra area).

[39] The oblique relative motion in Sumatra is partitioned between the Sunda trench and the Great Sumatran Fault [McCaffrey, 1991; Prawirodirdjo *et al.*, 1997; Bellier *et al.*, 1999; Duquesnoy *et al.*, 1999; McCaffrey *et al.*, 2000; Genrich *et al.*, 2000; Bock *et al.*, 2003]. The computed strain rates (Figure 3) show a deformation compatible with right-lateral strike slip on the Great Sumatran Fault and a compression normal to the trench, in agreement with these previous results. GPS-derived slip rates on the Great Sumatran Fault increase from ~23 mm/yr at 0.8°S to ~26 mm/yr at 2.7°N [McCaffrey *et al.*, 2000; Genrich *et al.*, 2000]. These rates are compatible with geologic estimates to the north but are 10% higher to the south [Sieh and Natawidjaja, 2000; Bellier and Seberier, 1995]. Hence at 0° latitude ~42 mm/yr (oriented) N35° needs to be accommodated by the trench. Studies here using local geodetic data showed that the subduction zone is coupled (with the upper plate accumulating elastic deformation) and recognize that lateral variations exist [Prawirodirdjo *et al.*, 1997; Simoes *et al.*, 2004]. However, these models do not predict the significant deformation observed at up to 750 km away from the trench (compression axes in Figure 3 and velocity residuals at MEDA/SAMP, PHUK/PHKT, ARAU, and USMP in Figure 6). The GPS results here suggest that the deformed area is extremely large (up to Thailand and Malaysia) and evidently underestimated by Prawirodirdjo *et al.* [1997] and Simoes *et al.* [2004]. To test this hypothesis a simple dislocation model [Okada, 1985] was used to estimate the extent of elastic deformation from the trench on a plane trending N20° with a 13° dip angle (given by the focal mechanism of the 2004 Sumatra-Andaman earthquake [U.S. Geological Society (USGS), 2004]) and a 50 km locking depth (corresponding to a 220 km wide plane). It indeed predicts significant (>2mm/yr) elastic loading up to ~600 km from the trench (at 0°N). At MEDA in Medan, for example, 6 mm/yr (oriented) N21° is modeled against 6 mm/yr N36° measured. The small difference is due to the over simplified geometry used. There also appear to be significant lateral variations between 0° and 10°N in the (far field) strain accumulation, possibly related to changes in the trench direction (e.g., the west and north bends at 1°N and

3°N, respectively) and the transition of subduction of the Australian to subduction of the Indian plate (convergence rates at 6°N latitude of 50 mm/yr N3° (this paper) and 38 mm/yr N18° [Socquet *et al.*, 2006b], respectively). This could explain the relatively higher velocity residuals measured on Phuket Island PHUK/PHKT (Figure 6) that appear to be also affected by strike-slip motion on the Klong Mauri and/or Ranong fault zones in Thailand (Figure 7). At the latter fault, the largest shallow earthquake sequence with magnitudes 4.1 to 4.9 occurred in October 2006 near Chumporn station (BANH) and was most likely an aftermath result of the 2004 megathrust earthquake. To achieve a fully realistic model, a complete inversion of the real trench geometry requires both near and far field (3-D) high-accuracy geodetic data on Sumatra. With only local data the far reaching deformation was assumed zero or poorly constrained, leading to subduction models with only partial coupling (50%) [Prawirodirdjo *et al.*, 1997] or steep dip angles ( $20 \pm 5/3^\circ$ ) [Simoes *et al.*, 2004]. The far field data reveals the extent of the locked trench fault plane below Sundaland at a shallow dip angle  $\leq 13^\circ$  and full coupling on the subduction, which also matches the very large magnitude of the 2004 Sumatra-Andaman earthquake.

[40] South of Java island, the computed strain rates (Figure 3) show mostly pure compression, oriented NNE, perpendicular to the trench. Behind the subduction zone [Moore and Curray, 1980; Baroux *et al.*, 1998], significant strain rates with an oblique orientation affect the core of Java and are compatible with a left-lateral strike-slip fault cutting through the island. Between the Sunda Strait and Bali, the relative AU-SU motion remains oriented N14°  $\pm$  1° while increasing along the eastward curving Java trench. The trench normal rotates here gradually from N30° to N10° [McCaffrey, 1991] and hence normal convergence across the trench takes place at ~109–110°E longitude. Toward the west the convergence becomes increasingly oblique with the trench-parallel shear reaching ~17 mm/yr N300° south of western Java. A main fault in this part of Java is the Cimandiri Fault (CMF) [Newcomb and McCann, 1987; Malod *et al.*, 2004; Setyaji *et al.*, 1997]. The CMF has a left-lateral strike-slip motion (N70°) and takes up N-S compression at  $\pm 10$  mm/yr [Setyaji *et al.*, 1997]. This could explain the  $2.5 \pm 1.0$  mm/yr N295° (95% confidence level) residual motion of BAKO (Figure 6) located ~70 km N away from the CMF at the edge of the (volcanic) mountain range to the south relatively close to the plate boundary deformation zone.

[41] Toward Bali the convergence becomes oblique again (5° with a trench normal of 8°) and with shear now increasing in the opposite direction to ~6 mm/yr N98°. The kinematically determined “5° oblique” N13°  $\pm$  3° convergence azimuth (95% confidence level) here is still compatible with the “convergence” slip vector N3°  $\pm$  9° of McCaffrey [1991] but does favor left-lateral slip faulting. The steady azimuth of the relative motion shows convergence east of central Java becoming oblique again with little or no oblique slipping on the subduction thrust fault. Instead the remaining trench-parallel motion apparently is accommodated by one or more arc-oblique left-lateral NE-SW strike-slip faults originating in the fore arc possibly from trench-perpendicular compression and trench-parallel extension on the subduction interface. A steep increase of the

trench-normal to the west of central Java initially results in oblique thrusting [McCaffrey, 1992] at slip angles of  $N9^\circ \pm 8^\circ$  [McCaffrey, 1991] to  $N11^\circ \pm 4^\circ$  [Tregoning et al., 1994] (both averaged between  $105^\circ\text{E}$  and  $110^\circ\text{E}$ ) that are smaller than the estimated  $N14^\circ \pm 2^\circ$  plate convergence. The active CMF favors a possible explanation by left-lateral strike-slip faulting also on western Java [McCaffrey, 1991] and can be matched in the kinematic approximation if a constant clockwise offset of  $\sim 5^\circ$  between the trench-normal and the present azimuth of subduction [McCaffrey, 1992] is assumed. Hence the AU-SU motion southeast of Java reaches a larger obliquity of  $\sim 10^\circ$  accommodated by oblique left-lateral strike-slip faults that extend land inward and possibly continue throughout the island where many successive NE-SW fault strands exist (also near Yogyakarta) [Dardji et al., 1994; Hoffmann-Rothe et al., 2001]. The relative motions of BUTU and BALI with respect to Sundaland (Figure 6) support this along with observations on Java by Bock et al. [2003] (figure included in the electronic supplement), all showing E-W components that are unlikely to solely result from interseismic loading at the subduction interface. The computed strain rates in Figure 3 show very high strain rates (exceeding  $42 \times 10^{-9} \text{ yr}^{-1}$ ) mostly localized on the trench and thus indicate that the subduction (dip angle  $> 60^\circ$ ) is weakly coupled and does not transmit important elastic deformation inside the block.

#### 4.4.4. Sundaland/Australia/Philippine Triple Junction

[42] The Java trench evolves beyond  $120^\circ\text{E}$  from subduction zone to collision with the Australian plate along the Timor Trough [e.g., Moore and Curray, 1980; McCaffrey and Abers, 1991; Genrich et al., 1996; Villeneuve et al., 1998; Pubellier et al., 2003]. The collision resulted (Figure 3) in a broadly deformed area and affects the entire Molucca region. Situated at the triple junction of the Australian, Philippine, and Sundaland plates a complicated configuration of active plate boundaries is generated, characterized by very high strain rates and complex deformation.

[43] The Sulawesi island has been characterized by the rapid block-like rotation of the northeastern part in first approximation [Walpersdorf et al., 1998; Stevens et al., 1999; Simons et al., 2000; Bock et al., 2003]. Analysis of the dense Sulawesi subset (Figure 7) enables the identification of four microblocks (discussed in detail by Socquet et al. [2006a]). The northeastern part of Sulawesi comprises the North Sula (NS), East Sula (ES), and Manado (MA) blocks moving toward the NNW while rotating clockwise. In this area, the main compressive strain axis rotates anticlockwise (Figure 3) from NNE to NNW direction at the Minahassa trench in the north, to WNW direction at the Palu left-lateral strike-slip fault in the west of the island. In the southern part of Sulawesi the Makassar (MK) block rotates anticlockwise with the main compressive strain axis trending NNW. Contrary to Bock et al. [2003], stations here show significant (relative) motions of  $7\text{--}23 \pm 2.0 \text{ mm/yr}$  (95% confidence level) in N-NNW direction (Figure 6) and are not located on Sundaland. Instead they predict a tectonic closure rate of  $\sim 15 \text{ mm/yr}$  for the Makassar Strait between Sulawesi and Sundaland [Socquet et al., 2006a].

[44] West of Sulawesi, deformation at smaller but still significant rates extends into the northern and eastern parts of Borneo (Figure 6) where the detailed deformation patterns in Sabah, East Malaysia and around Brunei are

obtained from 6 years of continuous observations (MIRI, LABU, KINA, SAND, TAWX). Active deformation of northern Borneo is still poorly understood and active folds and thrusts along the western margin of north Borneo have been attributed to gravity sliding in the Crocker Range [Bol and Hoorn, 1980]. Rangin et al. [1999] suggested that crustal shortening at the NW Borneo Trench accommodates remnant E-W distributed motion of the Sundaland/Philippine (SU/PH) plate convergence. The residual motions of MIRI, LABU, KINA, SAND, TAWX, and TAWA (Figure 8) fit well a clockwise rotation (around a pole west of PUER) of the northern Borneo tip with small ( $< 1 \text{ mm/yr}$ ) internal deformation. Hence  $5 \pm 1 \text{ mm/yr}$  E-W shortening could be accommodated at the active NW Borneo Trench [Hinze et al., 1989] by mainly aseismic slip considering the low seismicity offshore of Sabah and Brunei, and southward on land by NW-SE running faults that initiate respectively south and north of the Mangkalihat peninsula [Moss and Wilson, 1998; Hall and Nichols, 2002]. The northerly fault along the Celebes Sea margin toward TAWA/TAWX is probably the offshore continuation of the Palu-Koro (left-lateral strike-slip) fault on Sulawesi [Socquet et al., 2006a], while the Sangkulirang fault [Moss and Wilson, 1998] runs in the direction of Brunei. Shallow seismicity (1973–2006) in Borneo (Figure 8) indicates both faults are active and suggests that the Sangkulirang fault extends “Trans-Borneo” to Brunei and absorbs NE-SW shortening across its southern (oblique-reverse) segment. However, impingement of the Mangkalihat peninsula by the north arm of Sulawesi would also cause higher seismic activity here and mark the beginning of collision in the Makassar Strait. Northeast of Sabah, seismic activity on the Sulu Trench ceases to the west of ZAMB (Mindanao Island) while focal mechanisms indicate strike-slip motion on the Sulu Ridge toward Sabah, normal motion along the east coast of Sabah, and strike-slip motion on the Tinjia fault in Sarawak (Figure 8). Therefore the entire northern tip of Borneo may (slowly) move independently with respect to Sundaland while remaining SU/PH plate convergence is absorbed at the NW Borneo Trench [Rangin et al., 1999]. Hereby the strike-slip faulting at the south coast of Sabah (Figure 8) may either also accommodate E-W shortening at the Celebes basin margin [Rangin et al., 1999] or instead result from the clockwise rotation of the northern tip of Borneo.

[45] To the south of the Mangkalihat peninsula internal deformation in the eastern margin of Borneo is characterized by E-W compression resulting from the counterclockwise rotation of the Makassar block and the subsequent closure of the Makassar Strait. On the basis of the above results and discussion it is clear that contrary to Bock et al.’s [2003] assumption, both Sulawesi and the northern part of Borneo do not belong to Sundaland.

## 5. Summary and Conclusion

[46] The velocity field for SE Asia presented here combines longer time series from a denser GPS network than all previous solutions. It has an unprecedented precision of  $\sim 1 \text{ mm/yr}$  at 95% confidence level, spans SE Asia entirely, and includes unpublished results for dense network subsets in Malaysia, Thailand, and Sulawesi. From the coupled analysis of the strain rates tensors and residual velocities, it

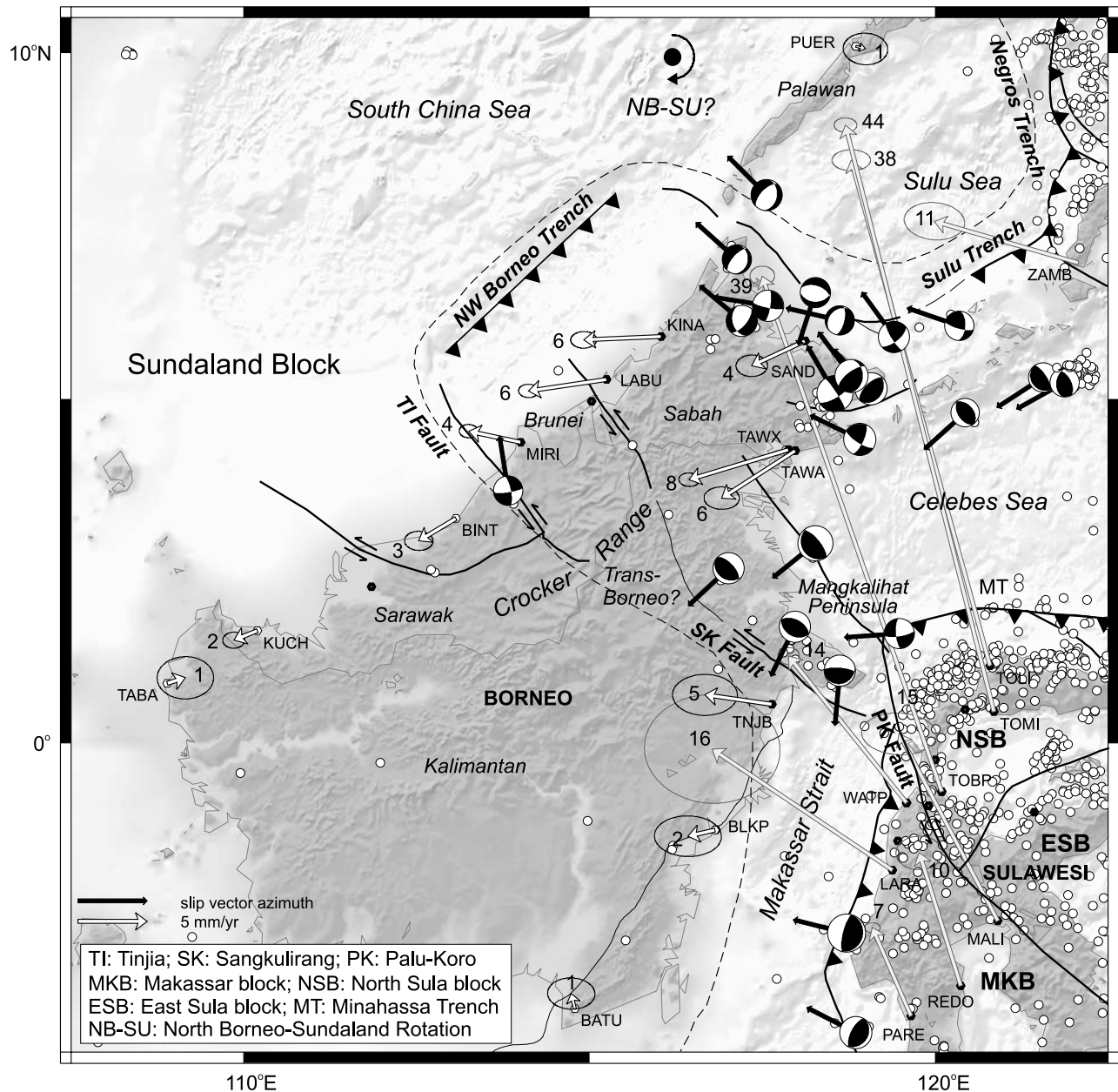


**Figure 8.** Velocities in Borneo with respect to Sundaland. The dashed line illustrates the boundaries of the undeformed Sundaland block. A small clockwise rotation of the tip of North Borneo can be deduced from the velocities (with the possible location of the NB-SU rotation pole plotted west of Palawan Island). The resulting left-lateral strike-slip motion is probably accommodated by the Tinjia and Sangkulirang faults of which the latter fault may run across the island. Faults on Borneo are based on *Moss and Wilson* [1998], *Hall and Nichols* [2002], and satellite images accessible through Google™ Earth. The historical seismicity (1973–2006) and the available moment tensor solutions (each included with preferred slip vector azimuth and slip direction toward Sundaland) [USGS, 2004] support the presence of active deformation on Borneo. The closure of the Makassar Strait is accommodated by subduction offshore the west coasts of Central and South Sulawesi.

was possible to localize a zone with very low strain rate and 28 residuals smaller than 3 mm/yr, which constitutes the “undeformed” core of the Sundaland block, which previously was only successfully detected with the GEODYSSSEA network. Densification of this network in combination with repeated measurements has resulted in better resolved Sundaland block boundaries and relative motions with respect to the surrounding tectonic region.

[47] The core of Sundaland covers Indochina, the Malaysian peninsula, the Sunda shelf, the southeastern part of Sumatra, the western and northern parts of Java, and the major part of Borneo. The block is bounded to the west by the Sagaing Fault in Myanmar, which connects to the Great Sumatran Fault through the Andaman pull-apart. To the south the boundaries are the Sunda trench and east of 110° E the Java strike-slip fault zone. To the east of Borneo the

Makassar Strait bounds Sundaland and excludes Sulawesi. The northern tip of Borneo is separated from Sundaland by "Trans-Borneo" faulting toward the active NW Borneo trench and offshore NW-SE faulting connecting to the Sulu Ridge. North of the Moluccas, the eastern boundaries of the Sundaland block are the Sulu, Negros, and Manila trenches located west of the Philippine islands. To the north, the limit is materialized by the deformation zone around the Eastern Himalayan Syntaxis and east of 103°E by the Red River fault with South China. Although the Sundaland block behaves as an independent tectonic entity, the high inter-plate deformation rates result in wide (>600 km) plate boundaries especially at the shallow subduction of the Australian plate below Sumatra. The common mode of deformation (1–3 mm/yr) within the Sundaland core is mainly due to elastic loading on the previously cited boundaries.

[48] The pole estimation confirms that the Sundaland block is rotating clockwise with respect to Eurasia (i.e., the GPS defined European-Siberian platform of *Calais et al.* [2003]) at a velocity of 6 to 9 mm/yr from south to north, respectively, or ~1–2 mm/yr faster if compared to Eurasia in NUVEL-1A-NNR. With respect to South China, Sundaland's motion is smaller (<5 mm/yr) but still significant and represented by a relative rotation pole lying close to their boundary, the Red River Fault. Therefore ~2 mm/yr right-lateral strike-slip motion is accommodated by the RRF east of 103°, accompanied by a transpressive component which decreases to almost zero in the South China Sea.

[49] Hence the Sundaland block is separated from the Siberian platform (still part of Eurasia) by at least one (the north and south China Block [e.g., *Calais et al.* 2003]) but probably two (Amuria/North China [e.g., *Petit and Fournier*, 2005] and South China [e.g., *Shen et al.*, 2005]) independent blocks. The presence of these microblocks confirms that the entire Asian continent mainly deforms in relation to the India-Eurasia collision. The new results show that at least far away from the collision zone itself, the lithosphere does not behave as a viscous medium but rather as rigid microblocks localizing the deformation along narrow fault zones. However, the results presented here also show that the motion accommodated by these faults, the Red River Fault in particular, is much smaller than expected by the extrusion model. Therefore it can be concluded that both crustal thickening in the region of the collision and extrusion of the East Asian blocks (Sundaland, South China, Amuria) contribute to plate tectonic interactions in the context of the India-Eurasia continental collision.

[50] **Acknowledgments.** This work is a continuation of joint EU-ASEAN research activities in SE Asia, initiated by the GEODYSSSEA project in 1991 and embedded in 2004 in the SEAMERGES-1 project (<http://www.deos.tudelft.nl/seamerges>) funded by the ASEAN- EU University Network Programme (AUNP). Thanks and appreciations are extended to ASEAN colleagues not visible in the author list who contributed to the expansion and analysis of the SE Asia GPS database. This applies particularly to the ITB students and BAKOSURTANAL surveyors in Indonesia for a decade of GPS measurements in Sulawesi, where support was also received (equipment and/or data) from the Scripps Institute of Oceanography and the Rensselaer Polytechnic Institute, US. The support for GPS activities from the Dutch Integrated Solid Earth Science (ISES) research program and the advice from the Jet Propulsion Laboratory on the GIPSY-OASIS software was greatly appreciated. Special thanks to Teruyuki Kato and Makiko Iwakuni of the Earthquake Research Institute in Tokyo and to the Geology department of Chulalongkorn University in

Bangkok for contributing permanent GPS data from Thailand, and Zheng-Kang Shen at the University of California, Los Angeles, for making additional South China rotation vector computations. This paper benefited from the constructive review by Paul Tregoning and anonymous reviewers, proofreading by David Lavalée and help with figures from Marc Naeije. Most figures in this paper were produced using the public domain Generic Mapping Tools (GMT). The Google™ Earth software has proved very useful to study fault traces in Borneo, Myanmar, and Thailand. The contents of this report are the sole responsibility of the authors listed and can under no circumstances be regarded as reflecting the position of the European Union. Finally, this work is dedicated to the memory of the 3 B.'s and S. who are dearly missed.

## References

- Allen, C., A. Gillespie, H. Yuan, K. Sieh, Z. Buchun, and Z. Chengnan (1984), Red River and associated Faults, Yunnan Province, China: Quaternary geology, slip rates, and seismic hazard, *Geol. Soc. Am. Bull.*, 95(6), 686–700.
- Altamimi, Z., P. Sillard, and C. Boucher (2002), ITRF2000: A new release of the International Terrestrial Reference Frame for earth science applications, *J. Geophys. Res.*, 107(B10), 2214, doi:10.1029/2001JB000561.
- Avouac, J. P., and P. Tapponnier (1993), Kinematic model of active deformation in Central-Asia, *Geophys. Res. Lett.*, 20(10), 895–898.
- Baroux, E., J. Avouac, O. Bellier, and M. Seberier (1998), Slip-partitioning and fore-arc deformation at the Sunda Trench, Indonesia, *Terra Nova*, 10(3), 139–144.
- Beavan, J., P. Tregoning, M. Bevis, T. Kato, and C. Meertens (2002), Motion and rigidity of the Pacific Plate and implications for plate boundary deformation, *J. Geophys. Res.*, 107(B10), 2261, doi:10.1029/2001JB000282.
- Bellier, O., and M. Seberier (1995), Is the slip rate variation on the Great Sumatran Fault accommodated by fore-arc stretching?, *Geophys. Res. Lett.*, 22(15), 1969–1972.
- Bellier, O., H. Bellon, M. Seberier, Sutanto, and R. Maury (1999), K-Ar age of the Ranau Tuffs: Implications for the Ranau caldera emplacement and slip-partitioning in Sumatra (Indonesia), *Tectonophysics*, 312(2–4), 347–359.
- Blewitt, G., et al. (1988), GPS geodesy with centimeter accuracy, in *GPS Techniques Applied to Geodesy and Surveying, Lecture Not. in Earth Sci.*, edited by E. Groten and R. Strauss, pp. 30–40, Springer-Verlag, New York.
- Bock, Y., L. Prawirodirdjo, J. Genrich, C. Stevens, R. McCaffrey, C. Subarya, S. Puntodewo, and E. Calais (2003), Crustal motion in Indonesia from Global Positioning System measurements, *J. Geophys. Res.*, 108(B8), 2367, doi:10.1029/2001JB000324.
- Bol, A. J., and B. V. Hoom (1980), Structural styles in Western Sabah offshore, *Bull. Geol. Soc. Malaysia*, 12, 1–16.
- Calais, E., M. Vergnolle, V. San'kov, A. Lukhnev, A. Miroshnichenko, S. Amargal, and J. Deverchere (2003), GPS measurements of crustal deformation in the baikal-Mongolia area (1994–2002): Implications for current kinematics of asia, *J. Geophys. Res.*, 108(B10), 2501, doi:10.1029/2002JB002373.
- Cardwell, R. K., and B. L. Isacks (1978), Geometry of the subducted lithosphere beneath the Banda Sea in Eastern Indonesia from seismicity and fault plane solutions, *J. Geophys. Res.*, 83, 2825–2838.
- Chamote-Rooke, N., and X. L. Pichon (1999), GPS determined eastward Sundaland motion with respect to Eurasia confirmed by earthquake slip vectors at Sunda and Philippine Trenches, *Earth Planet. Sci. Lett.*, 173, 439–455.
- Chen, Z., B. C. Burchfiel, Y. Liu, R. W. King, L. H. Royden, W. Tang, E. Wang, J. Zhao, and X. Zhang (2000), Global Positioning System measurements from eastern Tibet and their implications for India/Eurasia intercontinental deformation, *J. Geophys. Res.*, 105(16), 215–227.
- Curry, J., D. G. Moore, L. A. Lawver, F. J. Emmel, R. W. Raitt, M. Henry, and R. Kieckhefer (1979), Tectonics of the Andaman Sea and Burma: Geological and geophysical investigations of continental margins, *Am. Assoc. Petrol. Geol. Mem.*, 29, 189–198.
- Curry, J. C. (1989), The Sunda Arc: A model for oblique plate convergence, *Netherlands J. Sea Res.*, 24, 131–140.
- Dardji, N., T. Villemin, and J. P. Rampnoux (1994), Paleostress and strike-slip movement: The Cimandiri fault zone, west Java, Indonesia, *J. SE Asian Earth Sci.*, 9(1–2), 3–11.
- DeMets, C., R. Gordon, D. Argus, and S. Stein (1994), Effect of recent revisions to the geomagnetic reversal timescale on estimates of current plate motions, *Geophys. Res. Lett.*, 21, 2191–2194.
- Dixon, T. H., M. Miller, F. Farina, H. Wang, and D. Johnson (2000), Present-day motion of the Sierra Nevada block and some tectonic implications for the Basin and Range province, North American Cordillera, *Tectonics*, 19(1), 1–24.

- Duquesnoy, T., O. Bellier, M. Sebrier, M. Kasser, C. Vigny, F. Ego, I. Baha, E. Putranto, and I. Effendi (1999), Geodetic study of a seismic segment of the Great Sumatran Fault (Indonesia), *Bull. Soc. Geol. France*, *170*(1), 25–30.
- Earthquake Engineering Research Institute (2006), The Mw 6.3 Java, Indonesia, Earthquake of 27 May, 2006, special earthquake report, Oakland, Calif. (Available at [http://www.eeri.org/lfe/pdf/indonesia\\_java\\_eeri\\_prelim\\_report.pdf](http://www.eeri.org/lfe/pdf/indonesia_java_eeri_prelim_report.pdf))
- England, P., and G. Houseman (1986), Finite strain calculations of continental deformation: 2. Comparison with the India-Asia collision zone, *J. Geophys. Res.*, *91*(B3), 3664–3676.
- England, P., and P. Molnar (1997), Active deformation of Asia: From kinematics to dynamics, *Science*, *275*, 647–650, doi:10.1126/science.275.5338.647.
- Feigl, K. L., R. W. King, and T. H. Jordan (1990), Geodetic measurements of tectonic deformation in the Santa Maria Fold and Thrust Belt, *J. Geophys. Res.*, *95*(B3), 2679–2699.
- Feigl, K. L., D. C. Cong, M. Becker, T. D. To, K. Neumann, and N. Q. Xuyen (2003), Insignificant horizontal strain across the Red River Fault near Thac Ba, Vietnam from GPS measurements 1994–2000, *Geophys. Res. Abstr.*, *5*, 04707.
- Fenton, C. H., P. Charusiri, and S. H. Wood (2003), Recent paleoseismic investigations in Northern and Western Thailand, *Ann. Geophys.*, *46*(5), 957–981.
- Fernandes, R., B. Ambrosius, R. Noomen, L. Bastos, M. Wortel, W. Spakman, and R. Govers (2003), The relative motion between Africa and Eurasia as derived from ITRF2000 and GPS data, *Geophys. Res. Lett.*, *30*(16), 1828, doi:10.1029/2003GL017089.
- Fitch, T. J. (1972), Plate convergence, transcurrent faults, and internal deformation adjacent to Southeast Asia and the Western Pacific, *J. Geophys. Res.*, *77*(23), 4432–4460.
- Genrich, J., Y. Bock, R. McCaffrey, E. Calais, C. Stevens, and C. Subarya (1996), Accretion of the southern Banda arc to the Australian plate margin determined by Global Positioning System measurements, *Tectonics*, *15*(2), 288–295.
- Genrich, J., Y. Bock, R. McCaffrey, L. Prawirodirdjo, C. Stevens, S. Puntodewodli, C. Subarya, and S. Wdowinski (2000), Distribution of slip at the northern Sumatran fault system, *J. Geophys. Res.*, *105*(B12), 28,327–28,341.
- Gordon, R. G. (1995), Present plate motions and plate boundaries, in *Global Earth Physics: A Handbook of Physical Constants, Ref. Shelf. Ser., 1*, 66–87.
- Hall, R., and C. K. Morley (2004), Sundaland Basins, in *Continent-Ocean Interactions Within the East Asian Marginal Seas*, *Geophys. Monogr. Ser.*, vol. 149, edited by P. Clift et al., pp. 55–85, AGU, Washington, D. C.
- Hall, R., and G. J. Nichols (2002), Cenozoic sedimentation and tectonics in Borneo: Climatic influences on orogenesis, in *Sediment Flux to Basins: Causes, Controls and Consequences*, *Geol. Soc. London Spec. Publ.*, *191*, 5–22.
- Hamilton, W. (1979), Tectonics of the Indonesian region, *USGS Prof. Pap.*, *1078*, 345.
- Hinz, K., J. Fritsch, E. H. K. Kempter, A. M. Mohamad, J. M. J., D. Mohamed, H. Vosberg, and J. Weber (1989), Thrust tectonics along the north-western continental margin of Sabah/Borneo, *Geol. Rundsch.*, *139*, 705–730.
- Hoffmann-Rothe, A., O. Ritter, and V. Haak (2001), Magnetotelluric and geomagnetic modelling reveals zones of very high electrical conductivity in the upper crust of Central Java, *Phys. Earth Planet. Inter.*, *124*, 131–151.
- Holt, W. E., J. F. Ni, T. C. Wallace, and A. J. Haines (1991), The active tectonics of the eastern Himalayan syntaxis and surrounding regions, *J. Geophys. Res.*, *96*(B9), 595–632.
- Houseman, G., and P. England (1993), Crustal thickening versus lateral expulsion in the Indian-Asian continental collision, *J. Geophys. Res.*, *98*(B7), 12,233–12,249.
- Iwakuni, M., T. Kato, H. Takiguchi, T. Nakaegawa, and M. Satomura (2004), Crustal deformation in Thailand and tectonics of Indochina peninsula as seen from GPS observations, *Geophys. Res. Lett.*, *31*, L11612, doi:10.1029/2004GL020347.
- Kappel, E. S. (1980), Plate convergence in the Sunda and Banda arcs, 40 pp., B.A. thesis.
- King, R., F. Shen, B. Burchfiel, L. Royden, E. Wang, Z. Chen, Y. Liu, X. Zhang, J. Zhao, and Y. Li (1997), Global Positioning System measurements from eastern Tibet and their implications for India/Eurasia intercontinental deformation, *Geology*, *25*(2), 179–182.
- Kreemer, C., J. Haines, W. E. Holt, G. Blewitt, and D. Lavallee (2000), On the determination of a global strain rate model, *Earth Planets Space*, *52*, 765–770.
- Kreemer, C., W. Holt, and J. Haines (2003), An integrated global model of present-day plate motions and plate boundary deformation, *Geophys. J. Int.*, *154*, 8–34.
- Lacassin, R., A. Replumaz, and P. H. Leloup (1998), Hairpin river loops and slip-sense inversion on southeast Asian strike-slip faults, *Geology*, *26*(8), 703–706.
- Le Dain, A. Y., P. Tapponnier, and P. Molnar (1984), Active faulting and tectonics of Burma and surrounding regions, *J. Geophys. Res.*, *89*(B1), 453–472.
- Leloup, P., R. Lacassin, P. Tapponnier, U. Scharer, D. Zhong, X. Liu, L. Zhang, S. Ji, and P. Trinh (1995), The Ailao Shan-Red River shear zone (Yunnan, China), Tertiary transform boundary of Indochina, *Tectonophysics*, *251*(1–4), 3–84.
- Mader, G. (1998), GPS antenna calibration at the National Geodetic Survey, technical report, Natl. Geod. Surv., Silver Spring, Md.
- Malod, J. A., K. Karta, M. O. Beslier, and M. T. Z. Jr. (2004), From normal to oblique subduction: Tectonic relationships between Java and Sumatra, *J. SE Asian Earth Sci.*, *12*(1–2), 85–93, doi:10.1016/0743-9547(95)00023-2.
- Mao, A., C. G. A. Harrison, and T. H. Dixon (1999), Noise in GPS Coordinate Time Series, *J. Geophys. Res.*, *104*, 2797–2816.
- McCaffrey, R. (1991), Slip vectors and stretching of the Sumatran fore arc, *Geology*, *19*(9), 881–884.
- McCaffrey, R. (1992), Oblique plate convergence, slip vectors, and forearc deformation, *J. Geophys. Res.*, *97*(B6), 8905–8915.
- McCaffrey, R., and G. Abers (1991), Orography in arc-continent collision: The Banda Arc and Western New Guinea, *Geology*, *19*(6), 563–566.
- McCaffrey, R., P. Zwick, Y. Bock, L. Prawirodirdjo, J. Genrich, C. Stevens, S. Puntodewo, and C. Subarya (2000), Strain partitioning during oblique plate convergence in northern Sumatra: Geodetic and seismologic constraints and numerical modeling, *J. Geophys. Res.*, *105*(B12), 28,363–28,376.
- Michel, G., et al. (2001), Crustal motion and block behaviour in SE-Asia from GPS measurements, *Earth Planet. Sci. Lett.*, *187*, 239–244.
- Michel, G. W., M. Becker, D. Angermann, C. Reigber, and E. Reinhard (2000), Crustal motion in E- and SE-Asia from GPS measurements, *Earth Planets Space*, *52*(10), 713–720.
- Molnar, P., and P. Tapponnier (1978), Active tectonics of Tibet, *J. Geophys. Res.*, *83*(B11), 5361–5375.
- Moore, G., and J. Curry (1980), Structure of the Sunda Trench lower slope off Sumatra from multichannel seismic-reflection data, *Mar. Geophys. Res.*, *4*(3), 319–340.
- Moss, S. J., and M. E. J. Wilson (1998), Biogeographic implications from the Tertiary palaeogeographic evolution of Sulawesi and Borneo, in *Biogeography and Geological Evolution of SE Asia*, pp. 133–155, Backhuys, Leiden, Netherlands.
- Newcomb, K. R., and W. R. McCann (1987), Seismic history and seismotectonics of the Sunda Arc, *J. Geophys. Res.*, *92*, 421–439.
- Noquet, J. M., and E. Calais (2003), Crustal velocity field of western Europe from permanent GPS array solutions, 1996–2001, *Geophys. J. Int.*, *154*(1), 72–88.
- Okada, Y. (1985), Surface deformation due to shear and tensile faults in a half space, *Bull. Seismol. Soc.*, *75*(4), 1135–1154.
- Peltzer, G., and F. Saucier (1996), Present-day kinematics of Asia derived from geologic fault rates, *J. Geophys. Res.*, *101*, 27,943–27,956.
- Petit, C., and M. Fournier (2005), Present-day velocity and stress fields of the Amurian Plate from thin-shell finite-element modelling, *Geophys. J. Int.*, *160*(1), 357–367, doi:10.1111/j.1365-246X.2004.02486.x.
- Pollitz, F. F., and T. H. Dixon (1998), GPS measurements across the northern Caribbean plate boundary: Impact of postseismic relaxation following historic earthquakes, *Geophys. Res. Lett.*, *25*, 2233–2236.
- Prawirodirdjo, L., and Y. Bock (2004), Instantaneous global plate motion model from 12 years of continuous GPS observations, *J. Geophys. Res.*, *109*, B08405, doi:10.1029/2003JB002944.
- Prawirodirdjo, L., et al. (1997), Geodetic observations of interseismic strain segmentation at the Sumatra subduction zone, *Geophys. Res. Lett.*, *24*(21), 2601–2604.
- Pubellier, M., J. Ali, and C. Monnier (2003), Cenozoic plate interaction of the Australia and Philippine Sea Plates: “Hit-and-run” tectonics, *Tectonophysics*, *363*(3–4), 181–199.
- Rangin, C. (1991), The Philippine Mobile Belt: A complex plate boundary, *J. SE Asian Earth Sci.*, *6*, 209–220.
- Rangin, C., X. L. Pichon, S. Mazzotti, M. Pubellier, N. Chamot-Rooke, M. Aurelio, A. Walpersdorf, and R. Quebral (1999), Plate convergence measured by GPS across the Sundaland/Philippine Sea plate deformed boundary: The Philippines and eastern Indonesia, *Geophys. J. Int.*, *139*, 296–316.
- Replumaz, A., R. Lacassin, P. Tapponnier, and P. Leloup (2001), Large river offsets and Plio-Quaternary dextral slip rate on the Red River fault (Yunnan, China), *J. Geophys. Res.*, *106*(B1), 819–836.
- Rhodes, B. P., R. Perez, A. Lamjuan, and S. Kosuwan (2004), Kinematics and tectonic implications of the Mae Kuang Fault, northern Thailand, *J. Asian Earth Sci.*, *24*(1), 70–89.

- Scherneck, H.-G. (1991), A parametrized solid Earth tide mode and ocean loading effects for global geodetic base-line measurements, *Geophys. J. Int.*, *106*(3), 677–694.
- Schoenbohm, L., B. C. Burchfiel, and C. Liangzhong (2006), Propagation of surface uplift, lower crustal flow, and Cenozoic tectonics of the southeast margin of the Tibetan Plateau, *Geology*, *34*(10), 813–816, doi:10.1130/G22679.1.
- Sella, G., T. Dixon, and A. Mao (2002), REVEL: A model for recent plate velocities from space geodesy, *J. Geophys. Res.*, *107*(B4), 2081, doi:10.1029/2000JB000033.
- Setyadj, B., I. Murata, J. Kahar, S. Suparka, and T. Tanaka (1997), Analysis of GPS measurement in West-Java, Indonesia, *Ann. Disas. Prev. Res. Inst. Kyoto Univ.*, *40*(B-1), 27–33.
- Shen, Z.-K., C. Zhao, A. Yin, Y. Li, D. D. Jackson, P. Fang, and D. Dong (2000), Contemporary crustal deformation in east Asia constrained by Global Positioning System measurements, *J. Geophys. Res.*, *105*(5), 721–734.
- Shen, Z. K., J. Lu, M. Wang, and R. Burgmann (2005), Contemporary crustal deformation around the southeast borderland of the Tibetan Plateau, *J. Geophys. Res.*, *110*, B11409, doi:10.1029/2004JB003421.
- Sieh, K., and D. Natawidjaja (2000), Neotectonics of the Sumatran fault, Indonesia, *J. Geophys. Res.*, *105*(B12), 28,295–28,326.
- Simoes, M., J.-P. Avouac, R. Cattin, and P. Henry (2004), The Sumatra subduction zone: A case for a locked fault zone extending into the mantle, *J. Geophys. Res.*, *109*, B10402, doi:10.1029/2003JB002958.
- Simons, W. J. F., B. A. C. Ambrosius, R. Noomen, D. Angermann, P. Wilson, M. Becker, E. Reinhart, A. Walpersdorf, and C. Vigny (1999), Observing plate motions in S. E. Asia: Geodetic results of the GEODYSSSEA project, *Geophys. Res. Lett.*, *26*(14), 2081–2084.
- Simons, W. J. F., D. L. F. van Loon, A. Walpersdorf, B. A. C. Ambrosius, J. Kahar, H. Z. Abidin, D. A. Sarsito, C. Vigny, S. H. Abu, and P. Morgan (2000), Geodynamics of S.E. Asia: First results of the Sulawesi 1998 GPS campaign, *IAG: Geod. Beyond 2000*, *121*, 271–277.
- Socquet, A., W. Simons, C. Vigny, R. McCaffrey, C. Subarya, D. Sarsito, B. Ambrosius, and W. Spakman (2006a), Microblock rotations and fault coupling in SE Asia triple junction (Sulawesi, Indonesia) from GPS and earthquake slip vector data, *J. Geophys. Res.*, *111*, B08409, doi:10.1029/2005JB003963.
- Socquet, A., C. Vigny, N. Chamot-Rooke, W. Simons, C. Rangin, and B. Ambrosius (2006b), India and Sunda plates motion and deformation along their boundary in Myanmar determined by GPS, *J. Geophys. Res.*, *111*, B05406, doi:10.1029/2005JB003877.
- Steblov, G., M. Kogan, R. King, C. Scholz, R. Burgmann, and D. Frolov (2003), Imprint of the North American plate in Siberia revealed by GPS, *Geophys. Res. Lett.*, *30*(18), 1924, doi:10.1029/2003GL017805.
- Stevens, C., R. McCaffrey, Y. Bock, J. Genrich, Endang, C. Subarya, S. Puntodewodli, Fauzi, and C. Vigny (1999), Rapid rotations about a vertical axis in a collisional setting revealed by the Palu fault, Sulawesi, Indonesia, *Geophys. Res. Lett.*, *26*(17), 2677–2680.
- Takiguchi, H., T. Kato, H. Kobayashi, and T. Nakaegawa (2000), GPS observations in Thailand for hydrological applications, *Earth Planet. Sci. Lett.*, *52*, 913–919.
- Tapponnier, P., and P. Molnar (1975), Major strike-slip faulting in China: Its significance for Asian tectonics, *Seismol. Soc. Am. Annu. Meet.*, *7*, 425–426.
- Tapponnier, P., and P. Molnar (1977), Active faulting and tectonics in China, *J. Geophys. Res.*, *82*(20), 2905–2930.
- Tapponnier, P., G. Peltzer, A. Y. Ledain, R. Armijo, and P. Cobbold (1982), Propagating extrusion tectonics in Asia—New insights from simple experiments with plasticine, *Geology*, *10*(12), 611–616.
- Tregoning, P., F. Brunner, Y. Bock, S. Puntodewo, R. McCaffrey, J. Genrich, E. Calais, J. Rais, and C. Subarya (1994), First geodetic measurement of convergence across the Java trench, *Geophys. Res. Lett.*, *21*, 2135–2138.
- U.S. Geological Society (USGS) (2004), USGS fast moment tensor solution 2004 Sumatra-Andaman Earthquake, report. (Available at [http://www.neic.cr.usgs.gov/neis/eq\\_depot/2004/eq\\_41226/neic\\_lav\\_q.html](http://www.neic.cr.usgs.gov/neis/eq_depot/2004/eq_41226/neic_lav_q.html))
- Vigny, C., A. Socquet, C. Rangin, N. Chamot-Rooke, M. Pubellier, M.-N. Bouin, G. Bertrand, and M. Becker (2003), Present day crustal deformation around Sagaing Fault, Myanmar, *J. Geophys. Res.*, *108*(B11), 2533, doi:10.1029/2002JB001999.
- Vigny, C., et al. (2005), Insight into the 2004 Sumatra-Andaman earthquake from GPS measurements in southeast Asia, *Nature*, *436*, 201–206, doi:10.1038/nature03937.
- Villeneuve, M., J. Rehault, J. Cornee, C. Honthaas, and W. Gunawan (1998), Geodynamic evolution of eastern Indonesia from the Eocene to the Pliocene, *Compt. Rendus Acad. Sci. Paris*, *327*(5), 291–302.
- Wallace, L. M., C. Stevens, E. Silver, R. McCaffrey, W. Loratung, S. Hasiata, R. Stanaway, R. Curley, R. Rosa, and J. Taugaloidi (2004), GPS and seismological constraints on active tectonics and arc-continent collision in Papua New Guinea: Implications for mechanics of microplate rotations in a plate boundary zone, *J. Geophys. Res.*, *109*, B05404, doi:10.1029/2003JB002481.
- Walpersdorf, A., C. Vigny, P. Manurung, C. Subarya, and S. Sutisna (1998), Determining the Sula block kinematics in the triple junction area in Indonesia by GPS, *Geophys. J. Int.*, *135*, 351–361.
- Wang, E., B. C. Burchfiel, L. H. Royden, L. Chen, J. Chen, W. Li, and Z. Chen (1998), Late Cenozoic Xianshuihe-Xiaojiang, Red River, and Dali fault systems of southwestern Sichuan and central Yunnan, China, *Spec. Pap. Geol. Soc. Am.*, *327*, 108.
- Wang, Q., et al. (2001), Present-day crustal deformation in China constrained by Global Positioning System measurements, *Science*, *294*(5542), 574–577, doi:10.1126/science.1063647.
- Weissel, J. K. (1981), Magnetic lineations in marginal basins of the western Pacific, *Phil. Trans. R. Soc. London Ser. A*, *300*, 223–247.
- Weldon, R., K. Sieh, O. Zhu, Y. Han, J. Yang, and S. Robinson (1994), Slip rate and recurrence interval of earthquakes on the Hong He (Red River) fault, Yunnan, PRC, paper presented at International Workshop on Seismotectonics and Seismic Hazard in SE Asia. UNESCO, Hanoi.
- Williams, S. D. P., Y. Bock, P. Fang, P. Jamason, R. M. Nikolaidis, L. Prawirodirjo, M. Miller, and D. J. Johnson (2004), Error analysis of 27 continuous GPS position time series, *J. Geophys. Res.*, *109*, B03412, doi:10.1029/2003JB002741.
- Wilson, P., et al. (1998), Study Provides Data on Active Plate Tectonics in Southeast Asia Region, *Eos Trans. AGU*, *79*(45), 545–549.
- Zumberge, J., M. Heflin, D. Jefferson, M. Watkins, and F. Webb (1997), Precise point positioning for the efficient and robust analysis of GPS data from large networks, *J. Geophys. Res.*, *102*, 5005–5017.

S. Haji Abu, Department of Survey and Mapping Malaysia (DSMM), Kuala Lumpur, Malaysia.

B. A. C. Ambrosius, S. Matheussen, and W. J. F. Simons, Delft Institute of Earth Observation and Space Systems (DEOS), Faculty of Aerospace Engineering, Delft University of Technology, Kluyverweg 1, NL-2629 HS Delft, Netherlands. (wim.simons@lr.tudelft.nl)

P. Morgan, School of Computing, University of Canberra, Canberra, ACT, Australia.

C. Promthong, Royal Thai Survey Department (RTSD), Bangkok, Thailand.

D. A. Sarsito, Institute of Technology Bandung (ITB), Bandung, Indonesia.

A. Socquet, Institut de Physique du Globe de Paris (IPGP), Paris, France.

W. Spakman, Faculty of Earth Sciences, University of Utrecht, Utrecht, Netherlands.

C. Subarya, National Coordination Agency for Surveys and Mapping (BAKOSURTANAL), Cibinong, Indonesia.

C. Vigny, École Normale Supérieure (ENS), Paris, France.